Versatile fiber-reinforced hydrogels to mimic the microstructure and mechanics of human vocal-fold upper layers

Daniel Ferri-Angulo, Hamid Yousefi-Mashouf, Margot Michel, Anne Mcleer, Laurent Orgéas, Lucie Bailly, Jérôme Sohier

Statement of significance

Human vocal folds are outstanding vibrating soft living tissues allowing phonation. Simple physical models that take into account the histological structure of the vocal fold and recapitulate its mechanical features are scarce. As a result, the relations between tissue components, organisation and vibro-mechanical performances still remain an open question. We describe here the development and the characterization of fiber-reinforced hydrogels inspired from the vocal-fold microstructure. These systems are able to reproduce the mechanics of vocal-fold tissues upon realistic cyclic and large strains under various multi-axial loadings, thus providing a mimetic model to further understand the impact of the fibrous network microstructure in phonation.

Graphical Abstract

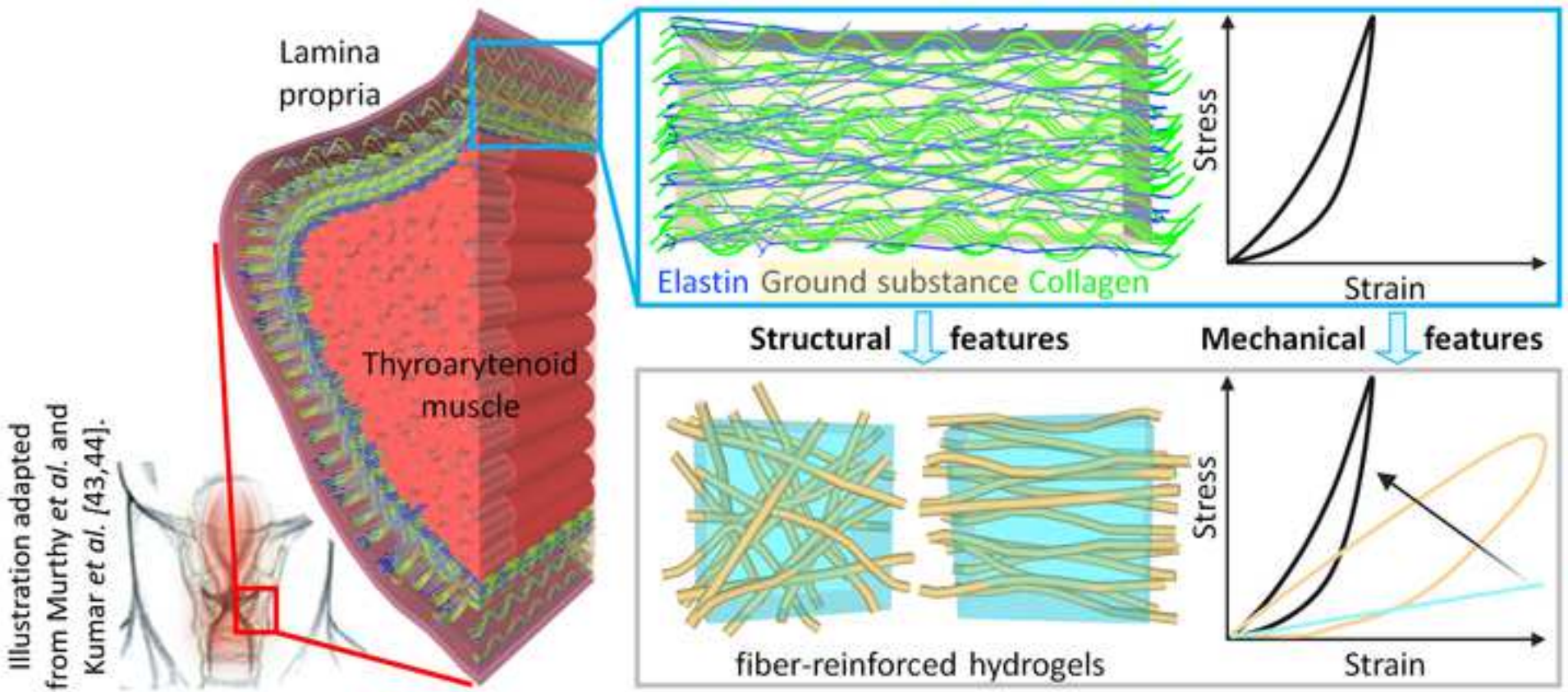

Versatile fiber-reinforced hydrogels to mimic the microstructure and mechanics of human vocal-fold upper layers

Daniel Ferri-Angulo*[a], Hamid Yousefi-Mashouf[b,c], Margot Michel[d], Anne McLeer[e], Laurent Orgéas[b], Lucie Bailly[†b], Jérôme Sohier[†§d]

[a]CNRS UMR5510 MATEIS, 7 Avenue Jean Capelle, F-69621, Villeurbanne, France
[b]Univ. Grenoble Alpes, CNRS, Grenoble INP, 3SR, 38000 Grenoble, France
[c]Univ. Grenoble Alpes, CNRS, Grenoble INP, GIPSA-lab, 38000 Grenoble, France
[d]CNRS UMR5305 LBTI, Passage du Vercors, 69007, Lyon, France
[e]Univ. Grenoble Alpes, Service d'Anatomie et Cytologie Pathologiques CHU Grenoble Alpes, Institute for Advanced Biosciences UGA/INSERM U1209/CNRS 5309, 38000 Grenoble, France

*Current affiliation: CNRS UPR8001 LAAS-TEAM, 7 Avenue Colonel Roche, 31031, Toulouse, France
[†]Contributed to this work equally
[§] Corresponding author: jerome.sohier@ibcp.fr

Keywords:

Vocal folds, Fiber-reinforced hydrogels, Materials by design, Two-photon excitation microscopy, Multiaxial mechanical characterization, Anisotropy, Viscoelasticity.

Abstract

Human vocal folds are remarkable soft laryngeal structures that enable phonation due to their unique vibro-mechanical performances. These properties are tied to their specific fibrous architecture, especially in the upper layers, which comprise a gel-like composite called *lamina propria*. The *lamina propria* can withstand large and reversible deformations under various multiaxial loadings. Despite their importance, the relationships between the microstructure of vocal folds and their resulting macroscopic properties remain poorly understood. There is a need for versatile models that encompass their structural complexity while mimicking their mechanical features. In this study, we present a candidate model inspired by histological measurements of the upper layers of human vocal folds. Bi-photonic observations were used to quantify the distribution, orientation, width, and volume fraction of collagen and elastin fibers between histological layers. Using established biomaterials, polymer fiber-reinforced hydrogels were developed to replicate the fibrillar network and ground substance of native

vocal fold tissue. To achieve this, jet-sprayed poly(ε-caprolactone) fibrillar mats were successfully impregnated with poly(L-lysine) dendrimers/polyethylene glycol hydrogels. The resulting composites exhibited versatile structural, physical and mechanical properties that could be customized through variations in the chemical formulation of their hydrogel matrix, the microstructural architecture of their fibrous networks (*i.e.*, fiber diameter, orientation and volume fraction) and their assembly process. By mimicking the collagen network of the *lamina propria* with polymer fibers and the elastin/ground substance with the hydrogel composition, we successfully replicated the non-linear, anisotropic, and viscoelastic mechanical behavior of the vocal-fold upper layers, accounting for inter/intra-individual variations. The development of this mimetic model offers promising avenues for a better understanding of the complex mechanisms involved in voice production.

1. Introduction

Human vocal folds are soft multi-layered laryngeal structures displaying remarkable mechanical performances [1,2]. These performances are primarily attributed to the unique properties of vocal-fold tissues, which allow them to endure large and reversible deformation under various multiaxial loading modes, including tension, compression and shear [3–5]. Furthermore, vocal folds exhibit the ability to adapt their vibro-mechanical behavior in response to environmental changes. These properties are related to the fibrous microstructures of the vocal folds and their surrounding gel-like matrices. In particular, the vocal-fold upper layers comprise a very thin *epithelium* surface and an underlying composite structure known as *lamina propria* (LP, thickness ≈ 1–2.5 mm; Fig. 1). The stratified squamous *epithelium* is secured to the LP through a basement membrane and serves as a protective covering [6]. The LP plays a crucial role in vocal-fold vibrations [7–9]. The LP is a loose connective tissue composed of cells and an extracellular matrix (ECM). This matrix includes an amorphous ground substance containing hyaluronic acid and is reinforced by entangled fibrous networks of collagen (mainly Type I and III) and elastin. As a whole, the LP significantly contributes to the mechanical properties of the upper layers, including non-linear viscoelasticity and anisotropy. More specifically, as schematized in Fig. 1, the mechanical strength and anisotropy of the LP are often ascribed to its collagen network, while its damping and elastic properties are more related to other tissue components (cells, elastic fibers, ground substances) [10,11].

Due to its physiological functions in voicing but also breathing and swallowing, the vocal-fold tissue has to accommodate many traumas (*e.g.,* vocal misuse or chemical aggression) [12,13]. Though characterized by an enhanced healing capacity of micro-lesions, the vocal-fold tissue can be damaged past a critical threshold of injury, resulting in benign lesions (*e.g.,* polyps, nodules [14]), or cancerous lesions (*carcinomas* [15]). Whatever the lesion, the LP microstructure is quasi-systematically altered, which induces dysfunctions in the vocal-fold vibro-mechanical performances. Current surgical procedures involve excision of the lesion or resection of the damaged tissue. However, in some complex cases, operative interventions can result in scarring lesions with partial disappearance of the LP layers and/or undesirable fibrous rearrangement, which may lead to the loss of phonatory abilities [16,17].

To treat these destructive lesions, several options are explored, including growth factor therapies, cell therapies and biomaterials, with the aim of rebuilding or replacing the layered structure of the *lamina propria* [13,16,18–24].

Among the relevant biomaterial candidates, hydrogels are attractive due to their tunable physical properties [25,26] and tissue-like water content [27–29], which provides cells with an environment comparable to the extracellular matrix of native tissues [30]. For instance, it has been shown that the implantation of hyaluronic acid (HA)-based hydrogels in the surgical wound maintains the superficial sublayer of the *lamina propria* and prevents the *epithelium* from adhering to the deeper sublayers during the healing process [31]. Similarly, injectable poly-ethylene glycol (PEG) polymers have also yielded positive vocal outcomes [32], albeit with limited effectiveness over time due to gradual material degradation. However, due to their isotropy and relatively low mechanical strength, homogeneous hydrogels may be limited in guiding tissue remodeling processes towards a native-like microstructure. The role of oriented fibrous microstructures and their anisotropic mechanics is increasingly recognized as a key factor influencing matrix synthesis, particularly in the case of elastin [33].

The mechanical features of native tissues are linked to their complex architecture, where fibrous protein networks support the hydrated ground substance [34]. Mimicking such a composite architecture through the reinforcement of hydrogels with fibrillar structures, as shown for cartilage, therefore appears as a promising concept to match target mechanical properties [35]. Many different models of various complexities have been proposed to better understand the phonatory ability of the vocal folds by reproducing their shape and multi-layered organization. However, these models are mostly made up of homogeneous elastomers with isotropic microstructures, resulting in quasi-linear stress-strain responses that differ significantly from those experienced by the vocal folds [36,37]. Over the last decade, a few promising *in vitro* developments have emerged to create composite elastomers aimed at mimicking the key microstructural features and anisotropic mechanical behavior of native vocal folds. For instance, Shaw *et al.* demonstrated that incorporating bundles of wavy polymeric fibers into isotropic self-oscillating silicone replicas could lead to a much more relevant fundamental frequency response, especially during anterior-posterior stretching [38]. Regarding biocompatible materials, a few examples able to mimic certain structural properties of the *lamina propria* have also been reported. Multi-layered hydrogels were

designed to promote cell viability and flow-induced vibrations [39], yet without taking into account the fibrous component of the native tissue. Other hydrogel scaffolds were developed from networks of collagen nanofibrils (Types I and III) in a glycol-chitosan matrix for vocal-fold tissue engineering [40]. However, their fibrous architecture, including diameter, orientation and density, was not tailored. Furthermore, the matching of their mechanical properties with those of the native tissue is rarely sought, which might render any potential mechanism of vibration difficult to translate to the native situation. Matching the mechanics of vocal fold models with those of native vocal folds has often been limited to a single loading mode, mainly shear, and to the linear regime at very small strains. These conditions are far from the cyclic and large-strain multiaxial loadings experienced by vocal folds during phonation [5]. The possibility of mimicking both the microstructural and quasi-static mechanical properties of the vocal fold under representative multi-axial loadings appears as a crucial first step towards a deeper investigation of the link between vocal-fold architecture and their mechanical vibration properties at higher strain rates.

The general objective of this work is twofold: (i) to develop and characterize hydrogels reinforced with tunable fibrous microstructures, inspired by quantitative histological data, and exhibiting versatile mechanical properties under both cyclic and finite strains; (ii) to identify among the proposed hydrogels those capable of replicating the major structural and mechanical specificities of the human vocal-fold upper layers, including longitudinal tension and transverse compression.

To achieve this, poly(ε-caprolactone) microfibers with adjustable densities and orientations [41,42] were embedded within a mimetic hydrogel. This hydrogel is composed of poly-lysine dendrimers and polyethylene glycol, offering highly modular mechanical properties [43]. This setup is schematically illustrated in Fig. 1. The structural and mechanical behavior of the resulting composites were characterized and compared to the histo-mechanical properties of native tissues.

2. Materials and method

2.1. Materials and sample preparation

2.1.1. Vocal folds

Histological experiments were carried out with one fresh healthy human larynx (no freezing step), excised from a donated body within 48 h *post-mortem* (male, 76-year-old).

Procedures were conducted following the French ethical and safety laws related to Body Donation. Right and left vocal folds were dissected along the longitudinal (anterior-posterior) direction $\boldsymbol{e}_{ap}$ (Fig. 1) using a dissection technique outlined by Bailly *et al.* [44]. The vocal folds were separated from their cartilaginous ends, resulting in four tissue samples, approximated as parallelepiped beams with dimensions of 10 mm × 3 mm × 3 mm.

These samples represent sandwich lamellar structures, encompassing all vocal-fold sublayers from the *epithelium* to the *vocalis* muscle (see Fig. 1). When possible, markers were sewn onto the samples, using Samco® surgical nylon monofilaments (10/0) and suture knots, to aid in anatomical identification during imaging experiments at the anterior end and within sublayers.

To enable high-resolution 3D imaging of their ECM fibers at the micrometer scale, a portion of the vocal-fold samples was immersed sequentially in ethanol (EtOH, Sigma-Aldrich) solutions with increasing alcohol concentration (30 %, 50 % and 70 %) for 24 h each. These samples were then stored in a 70 % EtOH solution at 4 °C until observation using two-photon microscopy. The other portion of the samples was fixed, embedded in paraffin and sectioned into 5 µm thick slices. These slices were either observed using two-photon microscopy or stained using conventional Hematoxylin-eosin-saffron (HES, in-house protocol) and Verhoeff Van Giesen (Labo Moderne, France). These stains were used to reveal both Type I and Type III collagen, as well as elastin fibers (see Supplementary Fig. S1). Stained sections were then imaged using an Aperio AT2 scanner (Leica, France).

2.1.2. Synthetic samples

PCL fibrous mats – In a first step, several mats made of poly(*ε*-caprolactone) (PCL, molecular weight 80,000 g/mol, Solvay Caprolactones, United Kingdom) microfibers with tunable orientation and volume fraction were prepared using a previously reported method, with modifications [41,42]. To make the PCL fibers hydrophilic, tween® 80 (245 mg, 187 mmol, Sigma-Aldrich, France) was stirred in chloroform (140 mL, Sigma-Aldrich, France) at room temperature (approximately 25 °C) for 10 min. Subsequently, PCL (9.8 g, 0.122 mmol) was added to the solution, and it was stirred for 3 h until complete dissolution occurred. The resulting solution was placed in a reservoir and projected onto different targets through the spraying device (standard class, Revell, Germany). Due to a Venturi effect, an airflow drove the polymer solution from the reservoir to an adjustable nozzle, where it was diffracted on a needle and sprayed. Solid polymer fibers were formed during transit due to chloroform evaporation. Two types of

targets were selected to create optional preferred orientations within the fibrous network, thereby allowing control over their induced mechanical properties. These targets included a static grid, which was used to produce mats with a planar random fiber orientation, and a rotating cylinder for fabricating mats with a planar fiber orientation featuring a preferred in-plane direction [41].

The thickness of the fibrous mats (was controlled by spraying time, and measured using a Keyence laser sensor. Typical values ranged within 0.5 to 3 mm. To increase the volume fraction of fibers, a compaction system was developed. Various levels of compaction were achieved by depositing one or multiple layers of fibrous mats of known thickness between layers of glass slats (each 0.14 mm thick). These layers were then covered by a glass plate and a 500 g weight was placed on top of the covering glass plate. Compaction was applied for 1 h at room temperature before release, new thickness measurement, and further use. Levels of compaction ranged from approximately 25 % up to 80 %, defined as the ratio of the relative change in thickness of the mat compared to its initial thickness.

DGL/PEG hydrogels – In a second step, hydrogels were obtained by mixing poly(L-lysine) dendrigrafts (DGL®, Colcom, France) and O,O′-Bis[2-(N-succinimidyl-succinylamino)ethyl] poly-ethylene glycol (PEG–NHS, Sigma-Aldrich, France) in aqueous solutions with various DGL/PEG ratios (1/1, 1/2, 1/2.5 or 1/3 w/w) and PEG molecular weights, referred to as PEG_{MW} (2 or 10 kDa). In a typical experiment, PEG–NHS in anhydrous dimethylformamide (DMF, Sigma-Aldrich, France) solution at different concentrations, noted C_{PEG} (5, 8, 10, 12 or 16 w/v %) was added to DGL in phosphate buffer saline (1x PBS, Euromedex, France) in eppendorf tubes at 4 °C. This mixture was swiftly vortexed and transferred to 3D-printed molds, where it cross-linked between 15 to 30 min at room temperature. After cross-linking, the hydrogels were removed from the mold and stocked in PBS solution at 4 °C until use. The resulting samples were typically 22 mm in length, 5 mm in width, and from 1 to 5 mm in thickness. In the following, for the sake of clarity, the DGL/PEG hydrogels characterized by the triplet of manufacturing parameters (C_{PEG} in %, PEG_{MW} in kDa, DGL/PEG ratio) will be denoted as Hyd(C_{PEG} %, PEG_{MW}k, DGL/PEG ratio).

Fiber-reinforced hydrogels – PCL fibrous mats, which had planar random or aligned orientations and were either compacted or not, were used along with DGL/PEG hydrogels to produce fiber-reinforced hydrogels. Each processed PCL mat was placed on a hydrophobic glass slide, and a fresh mix of PEG-NHS and DGL was rapidly poured onto it, allowing impregnation through the fibrous mats before the cross-linking reaction. Once the cross-linking was complete, the resulting composite samples were cut into parallelepiped beams measuring 22 mm in length, 5 mm in width and 0.5–2 mm in thickness. These composite materials were labelled FHC(C_{PEG} %, PEG_{MW}k, DGL/PEG ratio, fibrous orientation) and stored in PBS solution at 4 °C until use.

2.2. Structural, physical and mechanical characterization

2.2.1. Histological analyses of biological samples

The fibrous microstructure of the *lamina propria* samples was analyzed using two-photon excitation microscopy (Zeiss LSM 780) at the Cell Imaging Platform of the Cancer Research Center of Lyon (CRCL, UMR Inserm 1052 CNRS 5286 – Centre Léon Bérard, France). Samples conserved in a 70 %-ethanol solution were placed on a microscopy glass slide, moistened with PBS and covered by a glass coverslip, which was then sealed with patafix (UHU, Bühl, Germany) to prevent sample drying during observation. Collagen fibers were visualized using second harmony generation with an excitation at 900 nm and emission at 412–464 nm. For elastin, auto-fluorescence was utilized with an excitation at 900 nm and emission at 499–534 nm. When working with paraffin-embedded and sectioned samples, collagen fibers were observed via second harmony generation with an excitation at 900 nm and emission between 412 and 456 nm, while elastin autofluorescence was captured using an excitation at 700 nm and emission at 473–674 nm. Combining optics with CCD sensor features, regions of interest were sequentially scanned at multiple resolutions with effective voxel sizes of (0.69 µm × 0.69 µm × 6.17 µm), (0.35 µm × 0.35 µm × 0.91 µm) and (0.17 µm × 0.17 µm × 0.75 µm) in reference to the anatomical frame defined as ($\mathbf{e}_{ap}$, $\mathbf{e}_{ml}$, $\mathbf{e}_{is}$), where $\mathbf{e}_{ap}$ coincides with the anterior-posterior direction, $\mathbf{e}_{ml}$, with the medial-lateral direction, and $\mathbf{e}_{is}$ with the inferior-superior direction (see Fig. 1). The entire vocal-fold sample was examined in the ($\mathbf{e}_{ap}$, $\mathbf{e}_{ml}$) plane, with a maximum depth of 377 µm along the $\mathbf{e}_{is}$ direction. Stacks of images with distances of 6.17 µm, 0.91 µm and 0.75 µm were acquired along $\mathbf{e}_{is}$, resulting in thicknesses of 58.8 µm, 46.2 µm and 30.75 µm, respectively.

Distributions of diameter and 2D orientation of collagen and elastin fibers (parallel to the sample midplane) were calculated using the DiameterJ and OrientationJ plug-ins available in Fiji® [45,46]. For a acquisition stack, one $\mathbf{e}_{is}$-position was randomly selected at a depth of 22 µm, and six close-up areas of interest were analyzed to determine diameter and orientation populations, resulting in more than 6,000 values for each image. Additionally, to determine the diameter distribution of fiber bundles, manual quantification was performed at three random $\mathbf{e}_{is}$-positions within a given stack (depths of 15.3, 22 and 29.5 µm). Along the primary axis of each fiber bundle, a minimum of 10 orthogonal thickness measurements were recorded, resulting in more than 100 values for each image. Finally, to determine the volume fraction of collagen and elastin fibers in the tissue, the BoneJ plug-in available in Fiji® was utilized [47]. This involved manually thresholding three areas of interest from an acquisition stack for collagen and elastin signals, followed by the calculation of the volume ratio using the area/volume fraction algorithm.

2.2.2. Structural and physical characterization of synthetic samples

PCL fibrous mats – Jet-sprayed networks were observed by scanning electron microscopy (SEM, FEI XL30 ESEM-FEG, Philips, CLYM-INSA-Lyon, France) operated at a 2 kV accelerating voltage. Prior to observation, the fibers were coated with gold using a sputter coater (BAL-TEC SCD 005). For each sample, six SEM images were captured at random positions and different magnifications (×250, ×500 and ×2,000). Quantification of fiber diameters (more than 25,000 values for a given image) and orientations (more than 1,000 values for a given image) was performed in a manner similar to that employed for native tissue.

The porosity of the fibrillar mats ($\Phi_{PCL_{mats}}$) was determined, using a liquid displacement method with a pycnometer [48]. Ethanol served as the non-solvent working liquid, with a known density (ρ_{EtOH} = 0.7892 g/cm^3) [49]. The measurements involved weighing the fibrillary matrices (m_s) of 0.035 cm^3 (V_s), weighing the pycnometer filled with ethanol ($m_{py-EtOH}$) and the pycnometer containing both ethanol and the fibrillar sample (m_T). The porosity was calculated as follows:

$$\Phi_{PCL_{mats}} = 1 - \frac{\left(m_s + m_{py-EtOH}\right) - m_T}{\rho_{EtOH}\, V_s} \qquad (1)$$

All measurements were conducted in quintuplicate at 25 °C.

Hydrogels and fiber-reinforced composites – The morphology and structure of hydrogels and fiber-reinforced composites (FHC) were examined using a binocular microscope (Olympus, France).

Swelling ratio assays were performed to assess the water uptake and swelling properties of both materials. For hydrogels, the desired concentrations of DGL/PEG were mixed and the mixture promptly deposited between a hydrophobic glass slide and a hydrophobic round coverslip (10 mm in diameter) to create hydrogel disks after cross-linking. For FHC, the desired mixture of DGL/PEG was directly poured over fibrous mats cut as 10 mm-diameter disks. After cross-linking, the samples were immersed in PBS solution for 24 h at room temperature. Prior to freezing in liquid nitrogen, samples were washed with deionized water multiple times (8 × 1 h) and then freeze-dried, to measure their dry weight (w_d). Subsequently, the samples were immersed in PBS solution, and their swollen weight (w_s) was measured at various time intervals (ranging from 10 min to 48 h) after removing excess surface water. The swelling ratio (Q) was calculated for each sample using the formula:

$$Q = (w_s - w_d)/w_d \qquad (2)$$

The volume fraction of fibers in FHC samples (φ_{PCL}) was determined using a pycnometer [48], with PBS as working liquid. Composites were prepared with aligned or planar random fibrous mats of controlled volumes (V_s = 3.17 and 9.06 mm^3, respectively). The volume of the FHC samples, V_{FHC}, was calculated based on the weight of the composites (m_{FHC}), the weight of the pycnometer filled with both PBS and FHC samples (m_t), the PBS density (ρ_{PBS} = 1.002938 g/cm^3) and the known properties of the empty pycnometer (volume V_{py}, mass m_{py}) using the equation:

$$\varphi_{PCL} = \frac{V_s}{V_{FHC}} = \frac{V_s\,\rho_{PBS}}{V_{py}\,\rho_{PBS} - (m_t - m_{FHC} - m_{py})} \qquad (3)$$

For each of these data, four measurements were carried at 25 ◦C.

To determine the hydrogel mesh size (ζ), the rubber elastic theory was employed [50], where $\zeta = (G'/k_bT)^{-1/3}$, with G' as the shear storage modulus of the gel, k_b as the Boltzmann constant, and T as the temperature. Given the isotropic homogeneous cross-linking of PEG hydrogels, we set $G' = E/2(1+\nu)$, where E is the tensile elastic modulus, and ν the Poisson ratio [51,52]. Assuming quasi-incompressibility of the gel ($\nu \approx 0.5$), the mesh size

ζ was deduced from the tensile tests described below. Three measurements were used for mesh size determination.

2.2.3. Mechanical characterization

The mechanical response of PCL fibrous mats, DGL/PEG hydrogels and fiber-reinforced hydrogels was investigated using an electromechanical tension-compression testing machine (Instron® 5944) equipped with a load cell of ± 10 N (measurement accuracy ± 0.5 % of reading), following a protocol similar to that developed in Yousefi-Mashouf *et al.* [53] to characterize the mechanics of gelatin-based hydrogels. In particular, all tests were conducted in a thermo-regulated atmosphere (T ≈ 25 °C) and at proper hygrometric conditions to prevent samples from air drying: a dedicated hygro-mechanical set-up was used to maintain hydration of the gels in a saturated air atmosphere (≈ 98–100 % RH) throughout testing. Tests were repeated at least 5 times for each condition (Supplementary Fig. S2A showing the typical level of scatter in the measurements).

All materials were first characterized in tension along their main fiber orientation, which is the standard loading mode used to characterize the mechanical behavior of native tissues [54–57]. To do so, materials were cut in parallelepiped beams for an effective gauge length (ℓ_0) of 10 mm and width (w_0) of 5 mm. The initial thickness (t_0) of the samples could vary from 0.5 to 5 mm, depending on the sample nature and processing route. The maximum relative error obtained on the initial cross-section of the samples was estimated optically from their width and thickness profiles before loading using a high-resolution CCD camera (JAI® BM-500GE, 15 Hz), yielding to an error of ±0.02%. The cell force signal (f) and displacement of the machine cross-head (δ) were used to calculate the nominal stress ($P = f/w_0 t_0$) and the natural tensile strain ($\varepsilon = \ln(1 + \delta/\ell_0)$). Each sample was subjected to successive load/unload cycles with an increasing strain amplitude (ε^{max}) and a very low force at each unload phase for the inversion condition ($f >$ 5.10^{-3} N), with an initial strain rate $|\dot{\delta}/\ell_0| \approx 10^{-3}\, s^{-1}$.

To quantify the influence of cyclic loading, various mechanical descriptors were derived from the stress-strain curves [53], including the peak stress (P^{max}) achieved at every peak strain (ε^{max}); the residual strain (ε_r) recorded at the end of each cycle; the volumetric energy stored during the load of each cycle (W^{abs}) and the one dissipated after the unloading phase (W^{diss}); the corresponding energy dissipation coefficient ($\eta \approx W^{diss}/W^{abs}$) at the end of each cycle

[58]; and the tangent modulus ($E_t = dP/d\varepsilon$) assessed at the early stage of each unloading phase to capture the instantaneous stiffness of the material (with E= E_t at small strains).

In a second step, after comparison with the reference mechanical database on native tissues [5], a suitable biomimetic fiber-reinforced hydrogel candidate was selected from the previous campaign. It was further tested in compression transversely to the planar fiber orientation, such a loading being representative of vocal-fold loading during *in vivo* periodic collision [59,60]. Briefly, following the procedure developed in Yousefi-Mashouf *et al.* [53] in such a case, samples were cut for an effective gauge length ℓ_0 = 2 mm, a width and thickness w_0 = t_0 = 10 mm at rest. They were then subjected to successive load/unload cycles down to various strain levels (ε^{min}), with a strain rate ($|\dot{\varepsilon}|$) of approximately $10^{-3}\,s^{-1}$ as applied in the reference database. Compression stress (*P*) and strain (ε) were recorded during the test, as previously mentioned.

2.2.4. Statistical analysis

Statistical analyses were performed with OriginPro (OriginLab). After a Kolmogorov-Smirnov or Shapiro-Wilk normality test, parametric t-tests, variance analysis (ANOVA) or non-parametric Mann-Whitney U-tests were performed. P-values of 0.05 and below were considered significant.

3. Results and discussion

3.1. Structure of human vocal folds and lamina propria

Using two-photon microscopy, significant variations of collagen and elastin distributions across different histological layers of the human vocal folds were observed (Supplementary Fig. S1). Few collagen and elastin fibers were apparent in the *vocalis* muscle layer and arytenoid cartilage, while the *lamina propria* was rich in both types of fibers. In the *lamina propria*, both elastin and collagen fibers formed wavy structures, entangled in a network. As anticipated, the covering *epithelium* lacked these fibers (Fig. 2A). The predominant 2D orientation of the fibrillar proteins was parallel to the anterior-posterior direction ($\mathbf{e}_{ap}$), with density and orientation variations from the superficial to deep layers along the medial-lateral direction ($\mathbf{e}_{ml}$) (Fig. 2B and Supplementary Video S3).

Fig. 3 displays typical in-plane fiber orientation distributions and the width of ECM fibers measured at various depths of the *lamina propria*. In these in-plane analyses, both elastin and

collagen fibers intertwined networks showed a similar preferred orientation parallel to the anterior-posterior direction ($\mathbf{e}_{ap}$) (Fig. 3A). Close to the vocal fold's edge, beneath the *epithelium*, the angular distribution of fibers appeared broad, with the majority aligned parallel to the epithelial layer (θ = 0°). At deeper focal points within the *lamina propria*, the distribution of fibrillar orientation was narrower and predominantly followed the epithelial surface. When quantified through image analysis (Fig. 3B), collagen fibers were found to be significantly thicker, with broader dispersions (mean 2.1 ± 1.1 µm, median 1.7 µm, values ranging from 0.4 to 7.3 µm) compared to elastin ones (mean 1.4 ± 0.5 µm, median 1.4 µm and values ranging from 0.4 to 3.1 µm). Both fiber types formed bundles, which exhibited a similar pattern and reached widths of up to 94.1 and 62.9 µm. The mean values were 12.9 ± 12.1 µm (median 8.8 µm) for collagen and 9.9 ± 7.7 µm (median 7.8 µm) for elastin. Concerning the volume fractions of collagen and elastin fibers within the *lamina propria*, no significant different values were observed (9.7 ± 3.7 % and 10.9 ± 3.5 %, respectively; t-test p = 0.67). These findings are in good agreement with and complement the limited quantitative microstructural analyses of the human vocal fold reported in the existing literature [43,62,63]. Furthermore, our study indicated that using a larynx from a 76-year-old male did not result in significant differences in collagen and elastin fiber diameters and orientations when compared to those obtained from a 50-year-old female vocal fold using two-photon microscopy [62].

3.2. Tunable fiber-reinforced hydrogels

3.2.1. Structural and physical versatility

To approximate the observed microstructure of the native vocal-fold upper layers, several fiber-reinforced hydrogels (FHC) were developed. In this initial approach, the complex multi-layered structure of the upper layers was simplified into a one-layered composite structure.

The fibrillar component of the *lamina propria* can readily be emulated by polymeric materials, such as PCL, as they can be formulated in fibrous mats with controlled diameters, densities and orientations through various methods, including jet-spraying or electrospinning [42,63]). However, since the width of *lamina propria* ECM fibers is polydisperse, jet-spraying appeared to be a more suitable option to mimic this feature. Furthermore, this fiber production method results in highly porous structures, with a typical porosity around 97 %, which is a requisite to allow for the impregnation of a hydrogel phase for the creation of a composite.

By selecting jet-spraying parameters carefully, it was possible to emulate some of the target microstructural features of the *lamina propria* at the scale of fibers and fiber bundles. As presented in Fig. 4A, the in-plane orientation of the PCL fibers within the processed fibrous mats could be modulated to mimic the orientations of the fibrillar component observed in the *lamina propria* (Fig. 3). The resulting fibers diameters were in the micron range and significantly thicker when aligned, with averages of 2.9 ± 2.9 µm and 1.6 ± 1.4 µm, and medians of 1.9 µm and 1.2 µm for aligned and random mats, respectively. Similarly, the mean and median width of the fiber bundles produced during spraying were significantly increased, with means of 6 ± 5.6 µm compared to 3.2 ± 2.4 µm, and medians of 3.9 µm against 2.3 µm. In comparison to the measured collagen fibers of the *lamina propria*, mean diameters of both random and aligned fibrillar PCL mats were similar, but with a wider distribution. PCL fiber bundles diameters were also in the same order of magnitude as bundles of native fibrillar proteins, albeit with a lower mean and distribution range. It is worth noting that the polymer fibers obtained by jet-spraying did not reproduce the wavy pattern of collagen fibers of the *lamina propria* at the microscopic scale; instead, they appeared rather straight (see Fig. 4).

To replicate the remaining tissue components of the vocal-fold upper layers (*lamina propria* and *epithelium*), and to allow for control over the overall mechanical properties of the synthetic composites, a hydrogel of versatile properties was evaluated. In recent studies, we have demonstrated that poly(L-lysine) dendrigrafts/polyethylene glycol (DGL/PEG) hydrogels offer several advantages. These hydrogels can be easily prepared by mixing two aqueous solutions, and their elastic properties can be adjusted extensively by varying the component ratios and concentrations [43,64,65]. Importantly, unlike other PEG-based hydrogels, they exhibit inherent cytocompatibility, allowing for attachment and proliferation of multiple cell types *in vitro*, through the presence of DGL [43,65]. When implanted *in vivo*, these hydrogels are biocompatible, biodegradable and induce a mild inflammatory response, accompanied by extensive cellularization, tissue formation and vascularization [43]. The aqueous nature and low viscosity of PEG/DGL mixtures before cross-linking, along with the hydrophilicity imparted by the addition of tween® 80 to the PCL fibers, facilitated the impregnation of the hydrogel within the fibrous polymer mats through a simple pouring process. This resulted in a homogeneous impregnation throughout the thickness of the mats (see Fig. 5A). Moreover, due to the extremely high initial porosity of the mats ($\Phi_{PCL_{mats}}$ of 97 and 96 % for 2D aligned and 2D random mats, respectively), neither the orientation of the PCL fibers nor the

composition of the DGL/PEG hydrogel posed any obstacles to the preparation of the composites (FHC), as summarized in Table 1.

The efficient incorporation and embedding of fibrous mats within the hydrogels were evidenced in the modulation of their swelling properties. As presented in Fig. 5B, the increased swelling of DGL/PEG hydrogels under physiological conditions aligns with previously reported findings [43,65]. Increasing the PEG molecular weight (PEG_{MW}) from 2 to 10 kDa led to an increase in the swelling ratio from 15 to 22, whereas higher PEG concentration resulted in reduced water uptake by the hydrogels. Similarly to other PEG-based hydrogels, these effects can be attributed to the increased proximity of the amine (DGL) and NHS (PEG) reactive groups at higher reactants concentrations, leading to increased cross-linking, smaller mesh sizes and restricted network expansion [66]. In contrast, longer PEG chains resulted in larger mesh sizes and higher swelling, as indicated by the estimation of hydrogel mesh sizes (Table 1). However, for any given DGL/PEG composition and PEG molecular weight, the presence of PCL fibers significantly decreased the resulting FHC water uptake up to 3 times. This restriction in swelling can be attributed to the non-swelling nature of PCL fibers, as reported in previous studies on PEG-diglycidylether/polyoxyalkyleneamines hydrogels composites with polyurethanes fibers [67]. Additionally, this effect is influenced by the entangled organization of fibers in the non-woven jet-sprayed mats [42]. Accordingly, the swelling decrease was largely dependent on PCL fibers orientations and volume fractions in the final composite. In particular, the lower volume of hydrogel in the composites with random fibrous mats (≈ 91 %, compared to ≈ 96 % for aligned ones) induced a lower swelling ratio (Table 1).

Aside from the variation of fibers orientations and hydrogel composition, it was also possible to control the fiber content in the formed composites in a straightforward fashion. The elevated porosity of the fibrous mats permitted their relative compaction up to 80 % trough compression, while not hampering further impregnation with the hydrogel. As a result, the volume fraction of fibers φ_{PCL} within the resulting composites could be readily adjusted, as demonstrated in Fig. 5C for FHC(5%, 2k, 1/1, Aligned), where it increased from approximately 4 % up to about 16 %.

3.2.2. Tunable mechanical properties

Typical stress-strain responses – The cyclic tensile responses of the various elaborated materials are reported in Fig. 6, highlighting the differences in mechanical behavior between

each isolated component (DGL/PEG hydrogels and PCL fibrous mats) and the fiber-reinforced hydrogels, in the illustrative case of aligned fibers (see the case of 2D random fibers in Supplementary Fig. S2B).

In Fig. 6A, stress-strain curves for DGL/PEG hydrogels display quasilinear reversible behavior with minimal residual stress hysteresis. As anticipated [68,69], an increase in the PEG/DGL ratio led to higher stiffness (*e.g.,* tangent modulus E_t varying from 10 to 75 kPa for hydrogels with PEG_{MW} = 2 kDa at 5 % strain), while an increase in PEG_{MW} resulted in greater strains at break (from approximately 30 % to over 65 %). Accordingly, the softer hydrogel (*i.e.,* Hyd(10%, 10k, 1/2.5)) could hardly be manipulated and tested with the present protocol. In contrast, as shown in Fig. 6B, the processed fibrous mats exhibit elasto-plastic behavior, consistent with findings for raw PCL polymer and single PCL electrospun microfibers, which show irreversible deformation and necking past 5 % strain [70–72].

In the case of the composites (Fig. 6C–D and Supplementary Fig. S2), the incorporation of PCL fibers into the hydrogels consistently produced non-linear stress-strain responses characterized by J-shaped curves, likely resulting from the gradual reorientation of fibers along the tensile direction [70,73]. However, this strain hardening remains far less pronounced than that observed on isolated fibrous mats, due to the presence of the matrix, which constrains their kinematics to isochoric ones. Compared to non-reinforced hydrogels, stress levels achieved in the composites could be enhanced by up to two orders of magnitude in finite strains, in line with previous works on fiber-reinforced hydrogels [67,74] or other fiber-reinforced gel-like systems [75]. A typical stress hysteresis was also observed after each unloading sequence, resulting in non-zero residual strains. However, these residual strains were much less pronounced than those observed with fibers alone (see Fig. 6B and Supplementary Fig. S2B). This is ascribed to the elastic properties of the DGL/PEG matrix, which presumably limit the microstructural rearrangements (*e.g.,* fibers rotations and interactions) [11] and the large plastic deformation of the stretched PCL fibers. Finally, as anticipated, the strong anisotropy of the aligned fibrous mats was also reflected in the behavior of the composite (see Supplementary Fig. S2C).

Therefore, these global trends point out that the overall response of fibrous composites combines the high tensile strength, non-linear and anisotropic behavior of the fibrous mat upon finite strains (as ensured by collagen networks in native tissues), together with the elastic

recovery due to the cured homogeneous hydrogels (as induced by surrounding elastin and ground substance *in vivo*; Fig. 1).

Influence of the composite's formulation – Fig. 7 presents the strain-induced evolution of E_t, P^{max}, $W^{diss}$and ε_r related to FHC composites listed in Table 1.

Firstly, figures 6 and 7 highlights the effect of PEG molecular weight. Throughout the entire strain range studied (up to 40 %), composites with the lowest PEG_{MW} = 2 kDa showed higher tensile stiffness and peak strength (Fig. 7 A–B), in agreement with observations made for matrices alone (see Fig. 6A). These results align with the anticipated trends for hydrogels with shorter chains between chemical cross-links, as indicated by the corresponding shorter mesh sizes in Table 1. This suggests a higher cross-linker concentration [69]. Furthermore, beyond the early stage of deformation (for ε^{max} > 5 %), cyclic events with successive strain increments resulted in higher dissipated energy and lower residual strains in composites with the lowest PEG_{MW} (Fig. 7 C–D). Notably, this trend was not observed with neat hydrogels alone (see Fig. 6A). Hence, the observed changes in ε_r and W^{diss} with varying PEG_{MW} may be linked to structural rearrangements of PCL fibers within the composite (*e.g.,* rotations) and/or variations in fiber interfaces decohesion, likely influenced by matrix properties.

Secondly, Figures 6 and 7 also highlight the influence of the fiber content, a well-known key factor in the mechanics of fibrous materials [76,77]. This is particularly evidenced in the stress-strain responses of composites reported in Fig. 6D, the volume fraction of fibers φ_{PCL} of which from 0 % (neat gel) to 11 %, while keeping constant all other parameters (data shown here only for ε^{max} = 10 % for the sake of clarity). Furthermore, Fig. 8 clearly demonstrates that all the derived mechanical descriptors (E_t, P^{max}, η, ε_r) increased with φ_{PCL}, except for the residual strain ε_r which remained nearly constant for a given peak strain ε^{max}.

3.3. Towards the mechanical biomimetism of the vocal-fold upper layers

The structural properties of jet-sprayed PCL mats can be tuned to partially mimic collagen networks in the *lamina propria*. Additionally, the elastic moduli of PCL and collagen single fibrils fall within the same range (approximately from 500 MPa to 1 GPa [11,71,78]). These factors enabled us to propose a mechanical biomimicry of the human vocal-fold upper layers. However, it is important to note that, in this initial approach, fiber-reinforced hydrogels were developed to replicate the overall bulk mechanical properties of the vocal-fold upper layers, without distinguishing between the *epithelium* and the *lamina propria*. The mechanical

contribution of the micrometer-thick *epithelium* in the native sandwich composite structure was deemed negligible compared to the millimeter-thick, fiber-reinforced *lamina propria*.

Initially, from the various prepared composites, we selected a series of suitable candidates to replicate the visco-hyperelastic response of native tissues in longitudinal tension, aligning with the primary orientation of their collagen fibers. Specifically, in Fig. 9A, we illustrate the relevance of four composite hydrogels tuned to replicate samples of human vocal-fold upper layers (noted LP_1, LP_2, LP_3 to simplify labelling), which were subjected to comparable large-strains and cyclic uniaxial loads up to $\varepsilon^{max} \approx 10\%$ [5]. Such reference targets were extracted to define the typical range of mechanical responses observed *ex vivo* and to demonstrate the variability related to intra/inter-individual. Notably, LP_1 and LP_2 were obtained from left and right vocal folds of the same larynx. Previous studies have assessed the mechanical characteristics of human vocal fold tissue using various measurement techniques [79–81]. Here, our study endeavors to harmonize with data acquired from the same excised upper layers of human vocal fold subjected to a spectrum of physiological loading conditions [5]. This deliberate approach aimed at mitigating inherent variability arising from both inter/intra-individual differences and disparate measurement techniques. The mechanical descriptors (E_t, P^{max}, η, ε_r) relative to these target stress-strain behaviors are reported in Fig. 8.

This first selection was made among FHC composites with 2D preferred orientation. This choice aimed to induce structural and mechanical anisotropy close to those observed in living tissues. It also allowed for a wide distribution of orientations, allowing fiber rotation toward the load direction during tension. This micro-mechanism enable us to replicate the gradual recruitment of wavy collagen fibers during stretching of the *lamina propria* in the anterior-posterior direction [11]. Furthermore, composites with the lowest PEG_{MW} (2 kDa) were selected due to their increased stiffness and dissipative properties from small to finite strains, along with minimal residual strains after cycling. Specifically, as demonstrated in Fig. 8, the candidate FHC(5%, 2k, 1/1, Aligned) proved suitable for approximating the desired range represented by targets LP_i. This was achieved by adjusting φ_{PCL} values within the range of 3 % to 11 %, corresponding to the measured volume fraction of collagen fibers in the superficial *lamina propria* in our study (9.7 ± 3.7 %). Nonetheless, to match the softest target mechanical response (LP_1), a higher PEG_{MW} was necessary. For this specific case, the candidate FHC(12%, 10k, 1/3, Aligned) composed of the softest elaborated matrix (see Fig. 6A) was chosen.

In a second step, we evaluated the candidate FHC(5%, 2k, 1/1, Aligned) for suitability in transverse compression, *i.e.,* perpendicularly to the main fiber orientation. This loading mode is also very important during phonation, keeping in mind that the quality of contact between vocal folds is a key factor in voice quality, and that high contact pressure are observed in common lesions of the *lamina propria* [14,82]. In the end, as shown in Figs. 9A–B, the choice of $\varphi_{PCL} \approx 3$ % (in *green*) allowed the macroscale mechanics of the upper layers to be reproduced fairly well both in longitudinal tension and in transverse compression. In contrast to the trends observed in longitudinal tension, it is noteworthy that the response of the fibrous FHC composite under compression closely resembled that of that of the sole hydrogel matrix at low strains (see Fig. 9B), aligning with the characteristics of native vocal-fold tissue [11]. Additionally, it was observed that the mechanical contribution of the matrix in this mode decreased significantly for $\varepsilon < -0.05$, in line with predictions for biological tissue due to steric interactions likely occurring at the fiber scale [11].

4. Conclusion

In this study, we propose a set of versatile biocompatible fiber-reinforced hydrogels with tunable mechanical properties when subjected to cyclic and large-strains tensile and compressive loadings, such as those experienced by the *lamina propria* during human voice production. These composite hydrogels consist of jet-sprayed PCL fibrous mats embedded in a DGL/PEG matrix. The chemical formulation of their hydrogel matrix (*i.e.,* PEG molecular weight, concentration and DGL/PEG ratio), the microstructural architecture of their fibrous networks (*i.e.,* diameter, orientation and volume fraction of fibers) and their assembly process were tailored to ensure that the composites mimicked the anisotropic structure of the human upper layers (*i.e.,* the *lamina propria*, together with the very thin superficial *epithelium*), and its non-linear viscoelastic mechanical behavior. To do so, collagen and elastin fibrillar networks of deceased patients were characterized by two-photon excitation microscopy to quantify fiber and bundles diameters, preferential orientations and volume fractions, which, aside from providing concrete targets to match, completed the rare histological descriptors of the vocal fold. Using a recent mechanical database on native vocal-fold tissues subjected to longitudinal tension and transverse compression, the processed biomimetic composites were validated with respect to their non-linear strain hardening, mechanical strength, residual strain and

strain energy density dissipated during cycling. The versatility of the selected architectured materials was also highlighted, showing their ability to capture the dispersion of stress-strain responses related to inter or intra-individual variability. Overall, together with their potential to support cellularization and tissue formation *in vitro* and *in vivo*, the produced model materials allow to envision a better understanding of the role of the *lamina propria*'s structural characteristics in phonation under physiological aero-mechanical and acoustical loadings.

Acknowledgements

This work was supported by the French National Research Agency (ANR MicroVoice grant n° ANR-17-CE19-0015-01). The 3SR Lab is part of the LabEx Tec 21 (Investissements d'Avenir - grant agreement n° ANR-11-LABX-0030) and the Carnot PolyNat Institute (Investissements d'Avenir - grant agreement n° ANR-16-CARN-0025-01). We would like to thank Philippe Masson and Yohann Robert (Univ. Grenoble Alpes, CHU Grenoble Alpes, LADAF) for their helpful assistance in the excision of the biological samples. We also acknowledge Christophe Vanbelle (Centre Léon Bérard, CRCL) and Baptiste Robbiani (UMR 5510, MATEIS) for their technical support to the two-photon excitation microscopy and the estimation of hydrogel mesh sizes, respectively.

Conflict of interest statement

The authors declare no conflict of interest.

References

[1] M. Hirano, Morphological Structure of the Vocal Cord as a Vibrator and its Variations, Folia Phoniatrica et Logopaedica. 26 (2009) 89–94. https://doi.org/10.1159/000263771.

[2] I.R. Titze, Principles of voice production, National Center for Voice and Speech, Iowa City, Ia, 2000. http://books.google.com/books?id=ytAeAQAAMAAJ.

[3] A.K. Miri, Mechanical Characterization of Vocal Fold Tissue: A Review Study, Journal of Voice. 28 (2014) 657–667. https://doi.org/10.1016/j.jvoice.2014.03.001.

[4] T. Vampola, J. Horáček, I. Klepáček, Computer simulation of mucosal waves on vibrating human vocal folds, Biocybernetics and Biomedical Engineering. 36 (2016) 451–465. https://doi.org/10.1016/j.bbe.2016.03.004.

[5] T. Cochereau, L. Bailly, L. Orgéas, N. Henrich Bernardoni, Y. Robert, M. Terrien, Mechanics of human vocal folds layers during finite strains in tension, compression and shear, Journal of Biomechanics. 110 (2020) 109956. https://doi.org/10.1016/j.jbiomech.2020.109956.

[6] S.D. Gray, CELLULAR PHYSIOLOGY OF THE VOCAL FOLDS, Otolaryngologic Clinics of North America. 33 (2000) 679–697. https://doi.org/10.1016/S0030-6665(05)70237-1.

[7] K. Zhang, T. Siegmund, R.W. Chan, A two-layer composite model of the vocal fold lamina propria for fundamental frequency regulation, Journal of the Acoustical Society of America. 122 (2007) 1090–1101. https://doi.org/10.1121/1.2749460.

[8] Z. Zhang, J. Neubauer, D.A. Berry, Aerodynamically and acoustically driven modes of vibration in a physical model of the vocal folds, J Acoust Soc Am. 120 (2006) 2841–2849. https://doi.org/10.1121/1.2354025.

[9] W. Jiang, X. Zheng, Q. Xue, Influence of vocal fold cover layer thickness on its vibratory dynamics during voice production, J Acoust Soc Am. 146 (2019) 369–380. https://doi.org/10.1121/1.5116567.

[10] C. Finck, Implantation d'acide hyaluronique estérifié lors de la microchirurgie des lésions cordales bénignes, (2008). https://orbi.uliege.be/handle/2268/142631.

[11] A. Terzolo, L. Bailly, L. Orgéas, T. Cochereau, N. Henrich Bernardoni, A micro-mechanical model for the fibrous tissues of vocal folds, Journal of the Mechanical Behavior of Biomedical Materials. 128 (2022) 105118. https://doi.org/10.1016/j.jmbbm.2022.105118.

[12] R.C. Branski, K. Verdolini, V. Sandulache, C.A. Rosen, P.A. Hebda, Vocal Fold Wound Healing: A Review for Clinicians, Journal of Voice. 20 (2006) 432–442. https://doi.org/10.1016/j.jvoice.2005.08.005.

[13] J.K. Kutty, K. Webb, Tissue engineering therapies for the vocal fold lamina propria, Tissue Eng Part B Rev. 15 (2009) 249–262. https://doi.org/10.1089/ten.TEB.2008.0588.

[14] A. Hantzakos, M. Remacle, F.G. Dikkers, J.-C. Degols, M. Delos, G. Friedrich, A. Giovanni, N. Rasmussen, Exudative lesions of Reinke's space: a terminology proposal, Eur Arch Otorhinolaryngol. 266 (2009) 869–878. https://doi.org/10.1007/s00405-008-0863-x.

[15] P. Schultz, Vocal fold cancer, European Annals of Otorhinolaryngology, Head and Neck Diseases. 128 (2011) 301–308. https://doi.org/10.1016/j.anorl.2011.04.004.

[16] L. Li, J.M. Stiadle, H.K. Lau, A.B. Zerdoum, X. Jia, S.L. Thibeault, K.L. Kiick, Tissue engineering-based therapeutic strategies for vocal fold repair and regeneration, Biomaterials. 108 (2016) 91–110. https://doi.org/10.1016/j.biomaterials.2016.08.054.

[17] P. Woo, J. Casper, R. Colton, D. Brewer, Diagnosis and treatment of persistent dysphonia after laryngeal surgery: a retrospective analysis of 62 patients, Laryngoscope. 104 (1994) 1084–1091. https://doi.org/10.1288/00005537-199409000-00007.

[18] M. Imaizumi, R. Nakamura, Y. Nakaegawa, B.T. Dirja, Y. Tada, A. Tani, T. Sugino, Y. Tabata, K. Omori, Regenerative potential of basic fibroblast growth factor contained in biodegradable gelatin hydrogel microspheres applied following vocal fold injury: Early effect on tissue repair in a rabbit model, Brazilian Journal of Otorhinolaryngology. 87 (2021) 274–282. https://doi.org/10.1016/j.bjorl.2019.09.003.

[19] R.S. Bartlett, S.L. Thibeault, R.S. Bartlett, S.L. Thibeault, Bioengineering the Vocal Fold: A Review of Mesenchymal Stem Cell Applications, in: Advances in Biomimetics, IntechOpen, 2011. https://doi.org/10.5772/13803.

[20] J.L. Long, D.K. Chhetri, Restoring voice, Science. 350 (2015) 908–909. https://doi.org/10.1126/science.aad7695.

[21] C. Ling, Q. Li, M.E. Brown, Y. Kishimoto, Y. Toya, E.E. Devine, K.-O. Choi, K. Nishimoto, I.G. Norman, T. Tsegyal, J.J. Jiang, W.J. Burlingham, S. Gunasekaran, L.M. Smith, B.L. Frey, N.V. Welham, Bioengineered vocal fold mucosa for voice restoration, Sci Transl Med. 7 (2015) 314ra187. https://doi.org/10.1126/scitranslmed.aab4014.

[22] M. Gugatschka, S. Ohno, A. Saxena, S. Hirano, Regenerative Medicine of the Larynx. Where are we Today? A Review, Journal of Voice. 26 (2012) 670.e7-670.e13. https://doi.org/10.1016/j.jvoice.2012.03.009.

[23] N. Wan-Chiew, M.M. Baki, M.B. Fauzi, Y. Lokanathan, M. Azman, In Vitro Evaluation of Biomaterials for Vocal Fold Injection: A Systematic Review, Polymers. 13 (2021) 2619. https://doi.org/10.3390/polym13162619.

[24] J. Cedervall, L. Ahrlund-Richter, B. Svensson, K. Forsgren, F.H.J. Maurer, D. Vidovska, S. Hertegård, Injection of embryonic stem cells into scarred rabbit vocal folds enhances healing and improves viscoelasticity: short-term results, Laryngoscope. 117 (2007) 2075–2081. https://doi.org/10.1097/MLG.0b013e3181379c7c.

[25] S. Bashir, M. Hina, J. Iqbal, A.H. Rajpar, M.A. Mujtaba, N.A. Alghamdi, S. Wageh, K. Ramesh, S. Ramesh, Fundamental Concepts of Hydrogels: Synthesis, Properties, and Their Applications, Polymers. 12 (2020) 2702. https://doi.org/10.3390/polym12112702.

[26] Q. Chai, Y. Jiao, X. Yu, Hydrogels for Biomedical Applications: Their Characteristics and the Mechanisms behind Them, Gels. 3 (2017) 6. https://doi.org/10.3390/gels3010006.

[27] K. Deligkaris, T.S. Tadele, W. Olthuis, A. van den Berg, Hydrogel-based devices for biomedical applications, Sensors and Actuators B: Chemical. 147 (2010) 765–774. https://doi.org/10.1016/j.snb.2010.03.083.

[28] K.Y. Lee, D.J. Mooney, Hydrogels for Tissue Engineering, Chem. Rev. 101 (2001) 1869–1880. https://doi.org/10.1021/cr000108x.

[29] A.S. Hoffman, Hydrogels for biomedical applications, Advanced Drug Delivery Reviews. 64 (2012) 18–23. https://doi.org/10.1016/j.addr.2012.09.010.

[30] C.A. DeForest, K.S. Anseth, Advances in bioactive hydrogels to probe and direct cell fate, Annu Rev Chem Biomol Eng. 3 (2012) 421–444. https://doi.org/10.1146/annurev-chembioeng-062011-080945.

[31] C.L. Finck, B. Harmegnies, A. Remacle, P. Lefebvre, Implantation of esterified hyaluronic acid in microdissected Reinke's space after vocal fold microsurgery: short- and long-term results, J Voice. 24 (2010) 626–635. https://doi.org/10.1016/j.jvoice.2008.12.015.

[32] S.S. Karajanagi, G. Lopez-Guerra, H. Park, J.B. Kobler, M. Galindo, J. Aanestad, D.D. Mehta, Y. Kumai, N. Giordano, A. d'Almeida, J.T. Heaton, R. Langer, V.L.M. Herrera, W. Faquin, R.E. Hillman, S.M. Zeitels, Assessment of canine vocal fold function after injection of a new biomaterial designed to treat phonatory mucosal scarring, Ann Otol Rhinol Laryngol. 120 (2011) 175–184. https://doi.org/10.1177/000348941112000306.

[33] L.A. Hughes, J. Gaston, K. McAlindon, K.A. Woodhouse, S.L. Thibeault, Electrospun fiber constructs for vocal fold tissue engineering: effects of alignment and elastomeric polypeptide coating, Acta Biomater. 13 (2015) 111–120. https://doi.org/10.1016/j.actbio.2014.10.039.

[34] A. Abbott, Cell culture: biology's new dimension, Nature. 424 (2003) 870–872. https://doi.org/10.1038/424870a.

[35] J. Visser, F.P.W. Melchels, J.E. Jeon, E.M. van Bussel, L.S. Kimpton, H.M. Byrne, W.J.A. Dhert, P.D. Dalton, D.W. Hutmacher, J. Malda, Reinforcement of hydrogels using three-dimensionally printed microfibres, Nat Commun. 6 (2015) 6933. https://doi.org/10.1038/ncomms7933.

[36] P.R. Murray, S.L. Thomson, Vibratory responses of synthetic, self-oscillating vocal fold models, J Acoust Soc Am. 132 (2012) 3428–3438. https://doi.org/10.1121/1.4754551.

[37] R.G.T. Romero, M.B. Colton, S.L. Thomson, 3D-Printed Synthetic Vocal Fold Models, Journal of Voice. 35 (2021) 685–694. https://doi.org/10.1016/j.jvoice.2020.01.030.

[38] S.M. Shaw, S.L. Thomson, C. Dromey, S. Smith, Frequency response of synthetic vocal fold models with linear and nonlinear material properties, J Speech Lang Hear Res. 55 (2012) 1395–1406. https://doi.org/10.1044/1092-4388(2012/11-0153).

[39] R.K. Tindell, M.J. McPhail, C.E. Myers, J. Neubauer, J.M. Hintze, D.G. Lott, J.L. Holloway, Trilayered Hydrogel Scaffold for Vocal Fold Tissue Engineering, Biomacromolecules. 23 (2022) 4469–4480. https://doi.org/10.1021/acs.biomac.1c01149.

[40] N. Latifi, M. Asgari, H. Vali, L. Mongeau, A tissue-mimetic nano-fibrillar hybrid injectable hydrogel for potential soft tissue engineering applications, Sci Rep. 8 (2018) 1047. https://doi.org/10.1038/s41598-017-18523-3.

[41] J. Sohier, I. Carubelli, P. Sarathchandra, N. Latif, A.H. Chester, M.H. Yacoub, The potential of anisotropic matrices as substrate for heart valve engineering, Biomaterials. 35 (2014) 1833–1844. https://doi.org/10.1016/j.biomaterials.2013.10.061.

[42] J. Sohier, P. Corre, C. Perret, P. Pilet, P. Weiss, Novel and simple alternative to create nanofibrillar matrices of interest for tissue engineering, Tissue Eng Part C Methods. 20 (2014) 285–296. https://doi.org/10.1089/ten.TEC.2013.0147.

[43] M. Carrancá, L. Griveau, N. Remoué, C. Lorion, P. Weiss, V. Orea, D. Sigaudo-Roussel, C. Faye, D. Ferri-Angulo, R. Debret, J. Sohier, Versatile lysine dendrigrafts and polyethylene glycol hydrogels with inherent biological properties: in vitro cell behavior modulation and in vivo biocompatibility, J Biomed Mater Res A. 109 (2021) 926–937. https://doi.org/10.1002/jbm.a.37083.

[44] L. Bailly, T. Cochereau, L. Orgéas, N. Henrich Bernardoni, S. Rolland du Roscoat, A. McLeer-Florin, Y. Robert, X. Laval, T. Laurencin, P. Chaffanjon, B. Fayard, E. Boller, 3D multiscale imaging of human vocal folds using synchrotron X-ray microtomography in phase retrieval mode, Sci Rep. 8 (2018) 14003. https://doi.org/10.1038/s41598-018-31849-w.

[45] N.A. Hotaling, K. Bharti, H. Kriel, C.G. Simon, DiameterJ: A validated open source nanofiber diameter measurement tool, Biomaterials. 61 (2015) 327–338. https://doi.org/10.1016/j.biomaterials.2015.05.015.

[46] Z. Püspöki, M. Storath, D. Sage, M. Unser, Transforms and Operators for Directional Bioimage Analysis: A Survey, Adv Anat Embryol Cell Biol. 219 (2016) 69–93. https://doi.org/10.1007/978-3-319-28549-8_3.

[47] M. Doube, M.M. Kłosowski, I. Arganda-Carreras, F.P. Cordelières, R.P. Dougherty, J.S. Jackson, B. Schmid, J.R. Hutchinson, S.J. Shefelbine, BoneJ: Free and extensible bone image analysis in ImageJ, Bone. 47 (2010) 1076–1079. https://doi.org/10.1016/j.bone.2010.08.023.

[48] C.C. Xu, R.W. Chan, Pore architecture of a bovine acellular vocal fold scaffold, Tissue Eng Part A. 14 (2008) 1893–1903. https://doi.org/10.1089/ten.tea.2007.0243.

[49] A. Kiziltay, A. Marcos-Fernandez, J. San Roman, R.A. Sousa, R.L. Reis, V. Hasirci, N. Hasirci, Poly(ester-urethane) scaffolds: effect of structure on properties and osteogenic activity of stem cells, J Tissue Eng Regen Med. 9 (2015) 930–942. https://doi.org/10.1002/term.1848.

[50] M. Rubinstein, R.H. Colby, Polymer Physics, 1st edition, Oxford University Press, Oxford ; New York, 2003.

[51] P.X. Ma, J. Elisseeff, Scaffolding In Tissue Engineering, CRC Press, Boca Raton, 2005.

[52] M.S.M. Alger, Polymer science dictionary, 2nd ed, Chapman & Hall, London, 1997.

[53] H. Yousefi-Mashouf, L. Bailly, L. Orgéas, N. Henrich Bernardoni, Mechanics of gelatin-based hydrogels during finite strain tension, compression and shear, Frontiers in Bioengineering and Biotechnology. 10 (2023). https://www.frontiersin.org/articles/10.3389/fbioe.2022.1094197.

[54] J.E. Kelleher, K. Zhang, T. Siegmund, R.W. Chan, Spatially varying properties of the vocal ligament contribute to its eigenfrequency response, Journal of the Mechanical Behavior of Biomedical Materials. 3 (2010) 600–609. https://doi.org/10.1016/j.jmbbm.2010.07.009.

[55] J.E. Kelleher, T. Siegmund, M. Du, E. Naseri, R.W. Chan, The anisotropic hyperelastic biomechanical response of the vocal ligament and implications for frequency regulation: A case study, J Acoust Soc Am. 133 (2013) 1625–1636. https://doi.org/10.1121/1.4776204.

[56] R.W. Chan, M. Fu, L. Young, N. Tirunagari, Relative contributions of collagen and elastin to elasticity of the vocal fold under tension, Ann Biomed Eng. 35 (2007) 1471–1483. https://doi.org/10.1007/s10439-007-9314-x.

[57] E. Goodyer, J.J. Jiang, E. Devine, A. Sutor, S. Rupitsch, S. Zorner, M. Stingl, B. Schmidt, Devices and Methods on Analysis of Biomechanical Properties of Laryngeal Tissue and Substitute Materials, Current Bioinformatics. 6 (n.d.) 344–361.

[58] B. Gadot, O. Riu Martinez, S. Rolland du Roscoat, D. Bouvard, D. Rodney, L. Orgéas, Entangled single-wire NiTi material: A porous metal with tunable superelastic and shape memory properties, Acta Materialia. 96 (2015) 311–323. https://doi.org/10.1016/j.actamat.2015.06.018.

[59] H.E. Gunter, Modeling mechanical stresses as a factor in the etiology of benign vocal fold lesions, J Biomech. 37 (2004) 1119–1124. https://doi.org/10.1016/j.jbiomech.2003.11.007.

[60] H. Bakhshaee, J. Young, J.C.W. Yang, L. Mongeau, A.K. Miri, Determination of strain field on the superior surface of excised larynx vocal folds using DIC, J Voice. 27 (2013) 659–667. https://doi.org/10.1016/j.jvoice.2013.05.009.

[61] A.K. Miri, U. Tripathy, L. Mongeau, P.W. Wiseman, Nonlinear Laser Scanning Microscopy of Human Vocal Folds, Laryngoscope. 122 (2012) 356–363. https://doi.org/10.1002/lary.22460.

[62] F. Benboujja, C. Hartnick, Quantitative evaluation of the human vocal fold extracellular matrix using multiphoton microscopy and optical coherence tomography, Sci Rep. 11 (2021) 2440. https://doi.org/10.1038/s41598-021-82157-9.

[63] M.J. Mochane, T.S. Motsoeneng, E.R. Sadiku, T.C. Mokhena, J.S. Sefadi, Morphology and Properties of Electrospun PCL and Its Composites for Medical Applications: A Mini Review, Applied Sciences. 9 (2019) 2205. https://doi.org/10.3390/app9112205.

[64] R. Debret, C. Faye, J. Sohier, P. Sommer, Polypeptide Derived from Tropoelastin and Biocompatible Material Comprising Same, 2017. https://patentscope.wipo.int/search/en/detail.jsf?docId=WO2017194761.

[65] L. Griveau, M. Lafont, H. le Goff, C. Drouglazet, B. Robbiani, A. Berthier, D. Sigaudo-Roussel, N. Latif, C.L. Visage, V. Gache, R. Debret, P. Weiss, J. Sohier, Design and characterization of an in vivo injectable hydrogel with effervescently generated porosity for regenerative

medicine applications, Acta Biomaterialia. 140 (2022) 324–337. https://doi.org/10.1016/j.actbio.2021.11.036.

[66] B. Unal, R.C. Hedden, Gelation and swelling behavior of end-linked hydrogels prepared from linear poly(ethylene glycol) and poly(amidoamine) dendrimers, Polymer. 47 (2006) 8173–8182. https://doi.org/10.1016/j.polymer.2006.09.048.

[67] A. Agrawal, N. Rahbar, P.D. Calvert, Strong fiber-reinforced hydrogel, Acta Biomaterialia. 9 (2013) 5313–5318. https://doi.org/10.1016/j.actbio.2012.10.011.

[68] J.S. Temenoff, K.A. Athanasiou, R.G. LeBaron, A.G. Mikos, Effect of poly(ethylene glycol) molecular weight on tensile and swelling properties of oligo(poly(ethylene glycol) fumarate) hydrogels for cartilage tissue engineering, J Biomed Mater Res. 59 (2002) 429–437. https://doi.org/10.1002/jbm.1259.

[69] M.L. Oyen, Mechanical characterisation of hydrogel materials, International Materials Reviews. 59 (2014) 44–59. https://doi.org/10.1179/1743280413Y.0000000022.

[70] A. Delp, A. Becker, D. Hülsbusch, R. Scholz, M. Müller, B. Glasmacher, F. Walther, In Situ Characterization of Polycaprolactone Fiber Response to Quasi-Static Tensile Loading in Scanning Electron Microscopy, Polymers (Basel). 13 (2021) 2090. https://doi.org/10.3390/polym13132090.

[71] D. Alexeev, N. Goedecke, J. Snedeker, S. Ferguson, Mechanical evaluation of electrospun poly(ε-caprolactone) single fibers, Materials Today Communications. 24 (2020) 101211. https://doi.org/10.1016/j.mtcomm.2020.101211.

[72] H. Mondésert, Anisotropic PCL electrospun scaffolds for soft tissue engineering : Elaboration, morphological and mechanical properties, 2020.

[73] L. Bailly, M. Toungara, L. Orgéas, E. Bertrand, V. Deplano, C. Geindreau, In-plane mechanics of soft architectured fibre-reinforced silicone rubber membranes, Journal of the Mechanical Behavior of Biomedical Materials. 40 (2014) 339–353. https://doi.org/10.1016/j.jmbbm.2014.09.012.

[74] K. Tonsomboon, A.L. Butcher, M.L. Oyen, Strong and tough nanofibrous hydrogel composites based on biomimetic principles, Mater Sci Eng C Mater Biol Appl. 72 (2017) 220–227. https://doi.org/10.1016/j.msec.2016.11.025.

[75] T. Laurencin, P.J.J. Dumont, L. Orgéas, S.L. Corre, F. Martoïa, S. Rolland du Roscoat, P. Laure, 3D real time and in situ observation of the fibre orientation during the plane strain flow of concentrated fibre suspensions, Journal of Non-Newtonian Fluid Mechanics. 312 (2023) 104978. https://doi.org/10.1016/j.jnnfm.2022.104978.

[76] J. Jang, J. Lee, Y.-J. Seol, Y.H. Jeong, D.-W. Cho, Improving mechanical properties of alginate hydrogel by reinforcement with ethanol treated polycaprolactone nanofibers, Composites Part B: Engineering. 45 (2013) 1216–1221. https://doi.org/10.1016/j.compositesb.2012.09.059.

[77] F. Martoïa, P.J.J. Dumont, L. Orgéas, M.N. Belgacem, J.-L. Putaux, On the origins of the elasticity of cellulose nanofiber nanocomposites and nanopapers: a micromechanical approach, RSC Adv. 6 (2016) 47258–47271. https://doi.org/10.1039/C6RA07176G.

[78] P. Dutov, O. Antipova, S. Varma, J.P.R.O. Orgel, J.D. Schieber, Measurement of Elastic Modulus of Collagen Type I Single Fiber, PLoS One. 11 (2016) e0145711. https://doi.org/10.1371/journal.pone.0145711.

[79] D.K. Chhetri, Z. Zhang, J. Neubauer, Measurement of Young's modulus of vocal folds by indentation, J Voice. 25 (2011) 1–7. https://doi.org/10.1016/j.jvoice.2009.09.005.

[80] J.E. Kelleher, T. Siegmund, M. Du, E. Naseri, R.W. Chan, Empirical measurements of biomechanical anisotropy of the human vocal fold lamina propria, Biomech Model Mechanobiol. 12 (2013) 555–567. https://doi.org/10.1007/s10237-012-0425-4.

[81] F. Alipour, S. Vigmostad, Measurement of vocal folds elastic properties for continuum modeling, J Voice. 26 (2012) 816.e21–29. https://doi.org/10.1016/j.jvoice.2012.04.010.

[82] F. Silva, T. Legou, P. Champsaur, A. Giovanni, A. Lagier, Contact Pressure Between the Vocal Folds in Reinke's Edema: Experimental Observations on an Excised Human Larynx, J Voice. 35 (2021) 931.e15-931.e20. https://doi.org/10.1016/j.jvoice.2020.02.020.

Versatile fiber-reinforced hydrogels to mimic the microstructure and mechanics of human vocal-fold upper layers

Daniel Ferri-Angulo*[a], Hamid Yousefi-Mashouf[b,c], Margot Michel[d], Anne McLeer[e], Laurent Orgéas[b], Lucie Bailly[†b], Jérôme Sohier[†§d]

[a]CNRS UMR5510 MATEIS, 7 Avenue Jean Capelle, F-69621, Villeurbanne, France
[b]Univ. Grenoble Alpes, CNRS, Grenoble INP, 3SR, 38000 Grenoble, France
[c]Univ. Grenoble Alpes, CNRS, Grenoble INP, GIPSA-lab, 38000 Grenoble, France
[d]CNRS UMR5305 LBTI, Passage du Vercors, 69007, Lyon, France
[e]Univ. Grenoble Alpes, Service d'Anatomie et Cytologie Pathologiques CHU Grenoble Alpes, Institute for Advanced Biosciences UGA/INSERM U1209/CNRS 5309, 38000 Grenoble, France

*Current affiliation: CNRS UPR8001 LAAS-TEAM, 7 Avenue Colonel Roche, 31031, Toulouse, France
[†]Contributed to this work equally
[§] Corresponding author: jerome.sohier@ibcp.fr

Figure 1: Synthetic approach followed to mimic the major structural and mechanical specificities of human vocal-fold *lamina propria* through the design of poly-lysine dendrimers and polyethylene glycol (DGL/PEG) hydrogels reinforced with tunable jet-sprayed polymer fibrous architectures. Top center illustration adapted from Murthy et al. and Kumar *et al.* [43, 44].

Figure 2: Structural analysis of human *lamina propria*. **(A)** Close view of the *epithelium* and *lamina propria* layers of a human vocal-fold cross-section where collagen (blue) and elastin (yellow) are visualized through second harmonic generation and autofluorescence, respectively (pixel size 0.17 µm × 0.17 µm). **(B)** Examples of the organization of collagen at various depths of the same *lamina propria* sample (top panel: voxel size 0.69 µm × 0.69 µm × 6.17 µm, thickness 58.8 µm; bottom panel: voxel size 0.17 µm × 0.17 µm × 0.75 µm, thickness 30.8 µm).

Figure 3: Quantitative analysis of the fibrous architecture in the human *lamina propria*. **(A)** Representative 2D micrograph at several depths of the lamina propria (collagen appears blue and elastin yellow, voxel size 0.17 µm × 0.17 µm × 0.75 µm) and in-plane angular distribution of the collagen and elastin fibers, defined relative to the *epithelium*. **(B)** Quantification of the diameters of collagen and elastin fibers and fiber bundles. Mann-Whitney U-test for fibers: U = 308, n1 = 6047, n2 = 1496, **** $p < 0.0001$ two-tailed. Mann-Whitney U-test for bundles: U = 80951, n1 = 461, n2 = 308, **** $p < 0.0001$ two-tailed.

Figure 4: Mats of random and aligned PCL fibers. **(A)** Representative SEM pictures and quantification of their 2D orientations. **(B)** Quantification of the diameters of random and aligned fibers and fiber bundles. Mann-Whitney U-test for fibers: U = 3.1E10, n1 = 165168, n2 = 168364, **** p < 0.0001 two-tailed. Mann-Whitney U-test for bundles: U = 3.6E10, n1 = 165168, n2 = 221722, **** p < 0.0001 two-tailed.

Figure 5: Characterization of 2D random and 2D aligned fiber-reinforced hydrogels (FHC). **(A)** Representative pictures of both composite types. **(B)** Swelling ratios of hydrogels prepared with 2 (top) and 10 kDa PEG (bottom) at different concentrations (C_{PEG} = 5 and 10 %) and their homogeneous composites obtained with 2D random and 2D aligned fibrous PCL mats. **(C)** Modulation of FHC volume fraction through pre-compaction of aligned fibrous mats. Data are mean ± SD (n=5).

Figure 6: Mechanical characterization of hydrogels, PCL mats and FHC samples. Typical cyclic tensile stress-strain response of **(A)** various DGL/PEG homogeneous hydrogels, **(B)** aligned PCL fibrous mats under longitudinal loading, and **(C-D)** FHC composites reinforced by aligned fibers: illustrative cases of **(C)** FHC(10%, 2k, 1/2, Aligned) as listed in Table 1, and **(D)** FHC (5%, 2k, 1/1, Aligned) with a volume fraction of fibers φ_{PCL} varying from 0 % to 11 %. Error bars represent the measurement uncertainty, including the dispersion of the data over 5 repeated tests (min-max values) and the inherent accuracy errors. Grey areas illustrate hysteresis loops leading to a dissipation of mechanical energy.

Figure 7: Evolution of the mechanical descriptors of the composite hydrogels in function of the applied peak strains ε^{max}: **(A)** tangent modulus, E_t; **(B)** peak stress level, P^{max}; **(C)** dissipated energy density per cycle, W^{diss}; **(D)** residual strain, ε_r.

Figure 8: Modulation of fiber volume fraction φ_{PCL} in aligned FHC through pre-compaction of fibrous mats to mimic human vocal-fold upper layers (*lamina propria* + *epithelium*). Tensile mechanical descriptors as a function of the applied peak strain, ε^{max}, set at 10, 20 or 30 % (*from smallest to largest symbol*): **(A)** tangent modulus, E_t; **(B)** peak stress level, P^{max}; **(C)** energy dissipation coefficient, η; **(D)** residual strain, ε_r. Data acquired on composites FHC(5%, 2k, 1/1, Aligned). Colored areas (in orange) represent the range of target values as derived from Fig. 9, owning identical matrix and fibrous orientation, but tailored values of φ_{PCL}.

Figure 9: Comparison with reference data acquired on human vocal folds. **(A)** Stress-strain responses of tailored FHC composite candidates and upper layers samples (*lamina propria* + *epithelium*) subjected to cyclic and finite-strains in longitudinal tension [5]. **(B)** Typical stress-strain response of

the composite FHC(5%, 2k, 1/1, Aligned) under transverse compression, as previously selected from the tension curves in **(A)** (curve in green). Comparison with the corresponding homogenous hydrogel without fibers, and reference data on vocal-fold upper layers (*lamina propria* + *epithelium*) [5].

Table 1. Average mesh size (ζ) of PEG hydrogels and volume fraction of fibers (φ_{PCL}) in the fiber-reinforced hydrogels. One-way Anova with Tukey's multiple comparison test Hyd(x%, 2k, x/x) versus (x%, 10k, x/x): ****: $p < 0.0001$, n = 3 per condition. T-test random versus aligned FHC composites: **: $p < 0.01$, ***: $p < 0.001$, n = 4 per condition.

Figure 1

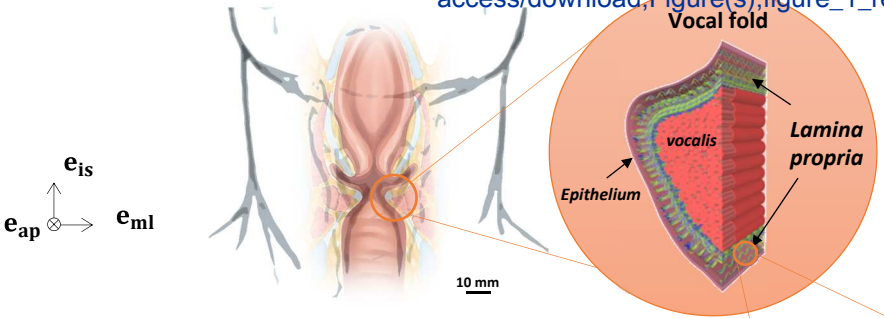

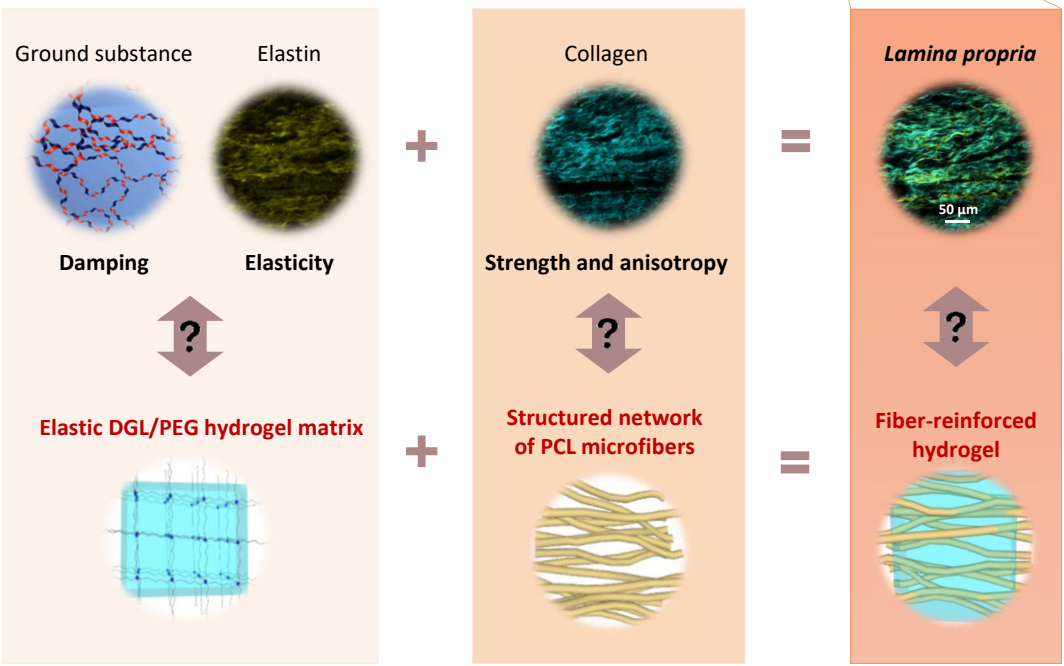

Figure 2

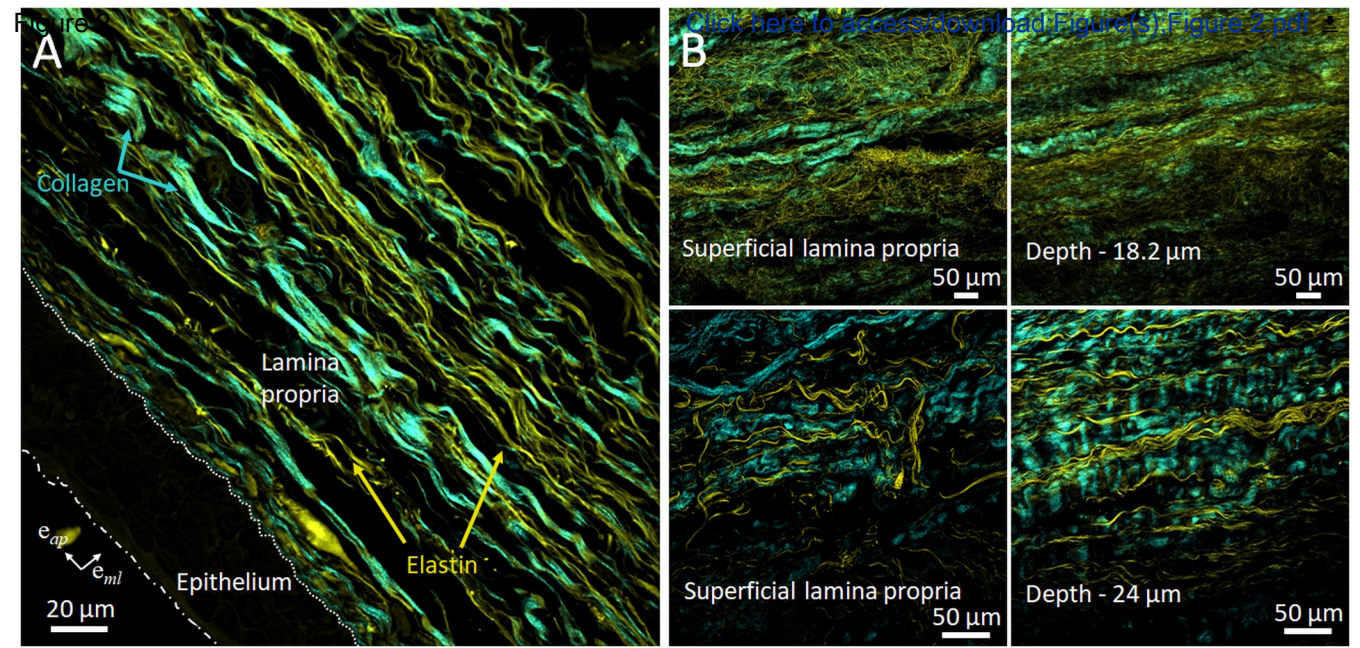

Figure 3

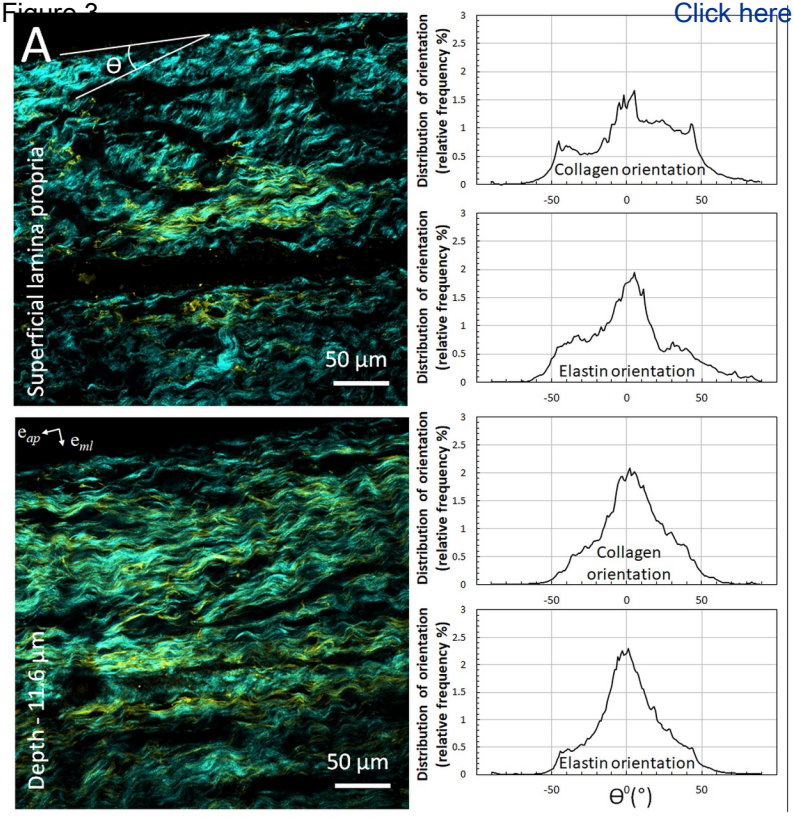

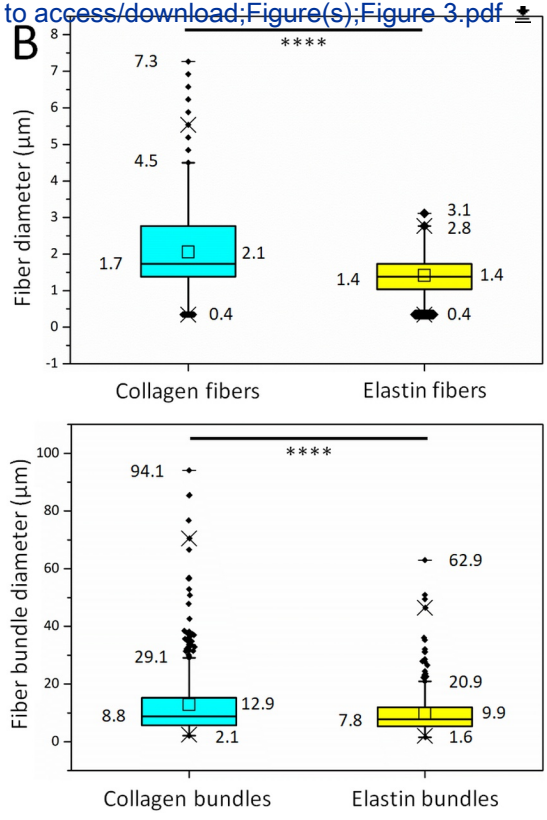

Figure 4

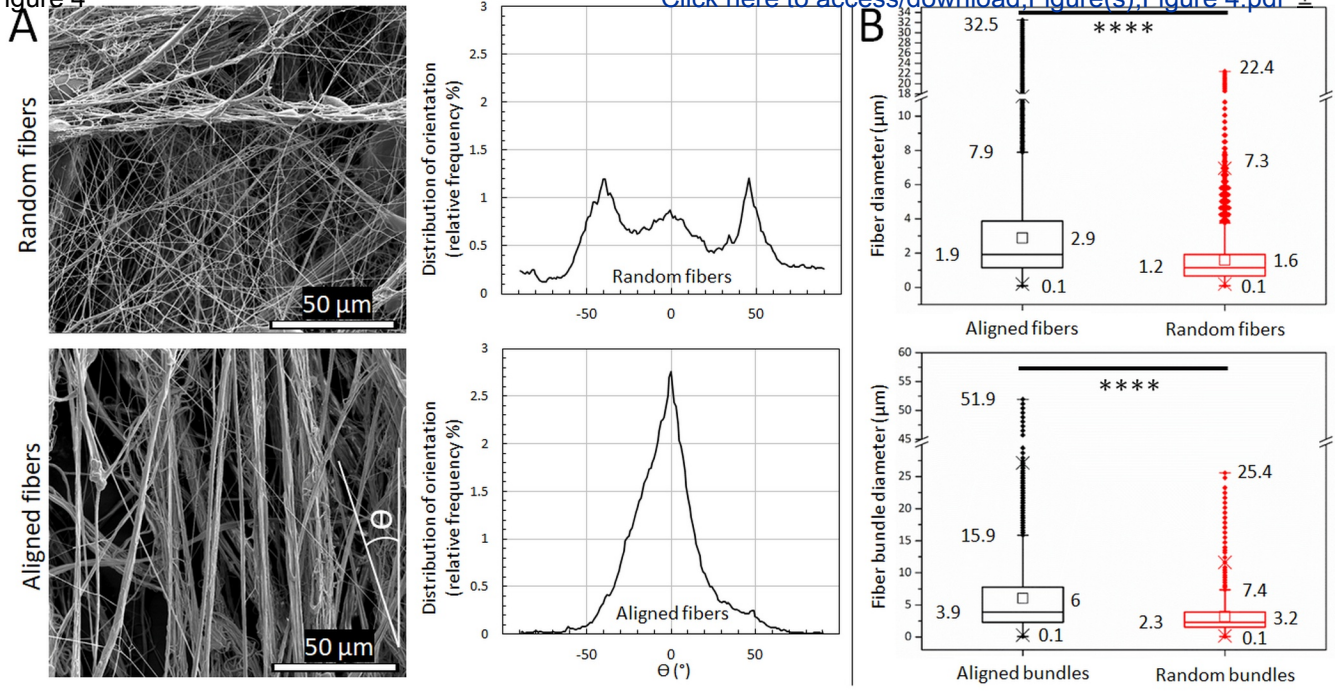

Figure 5

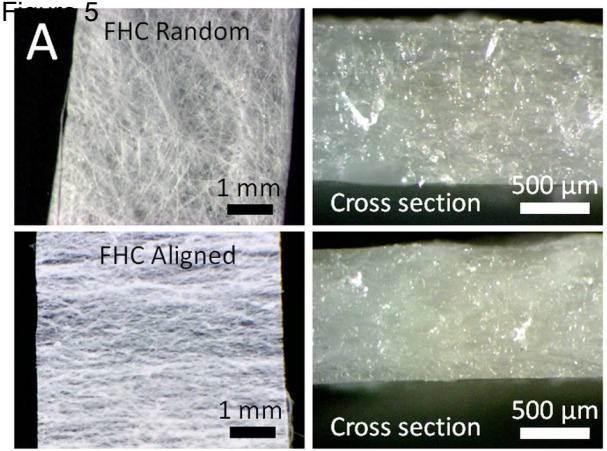

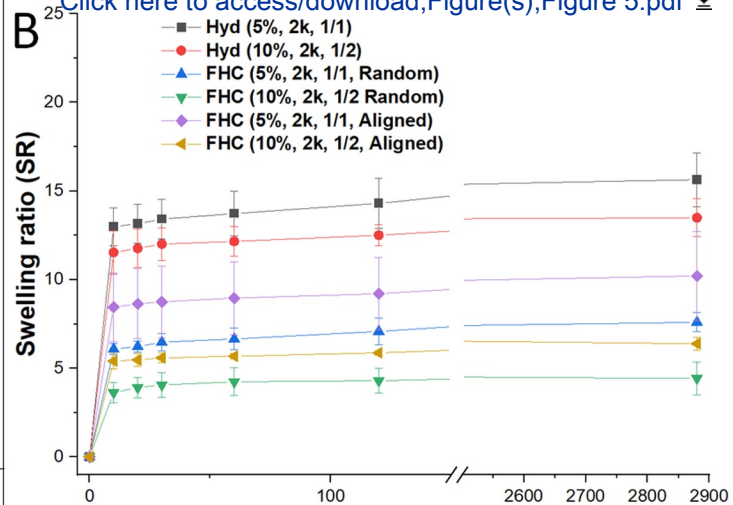

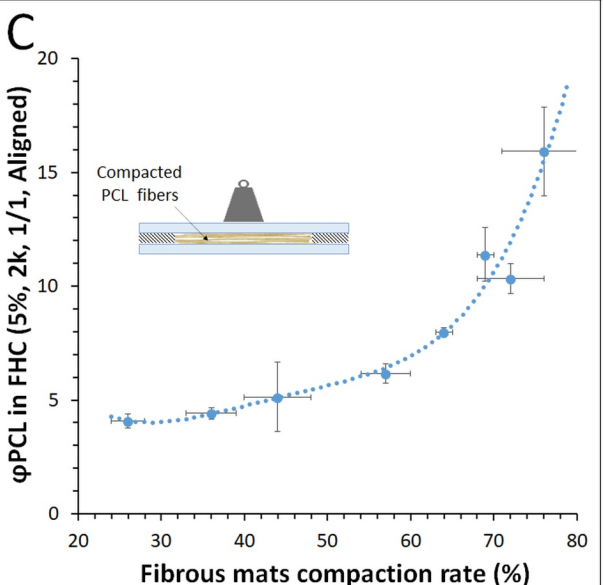

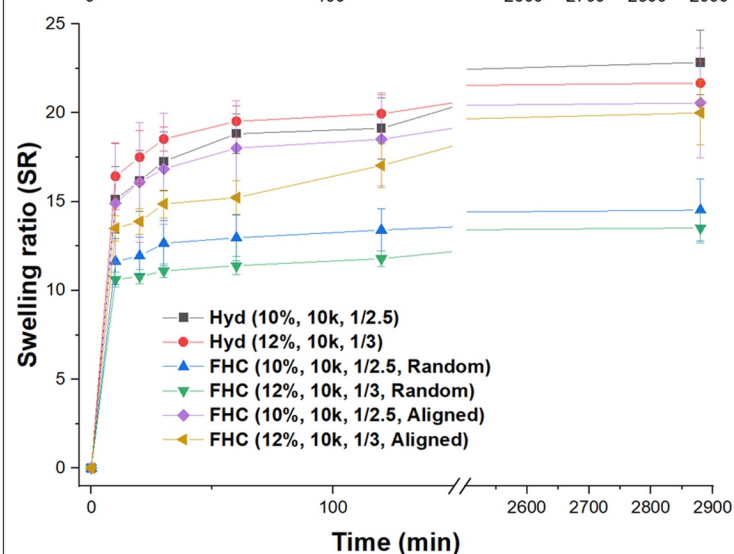

Figure 6

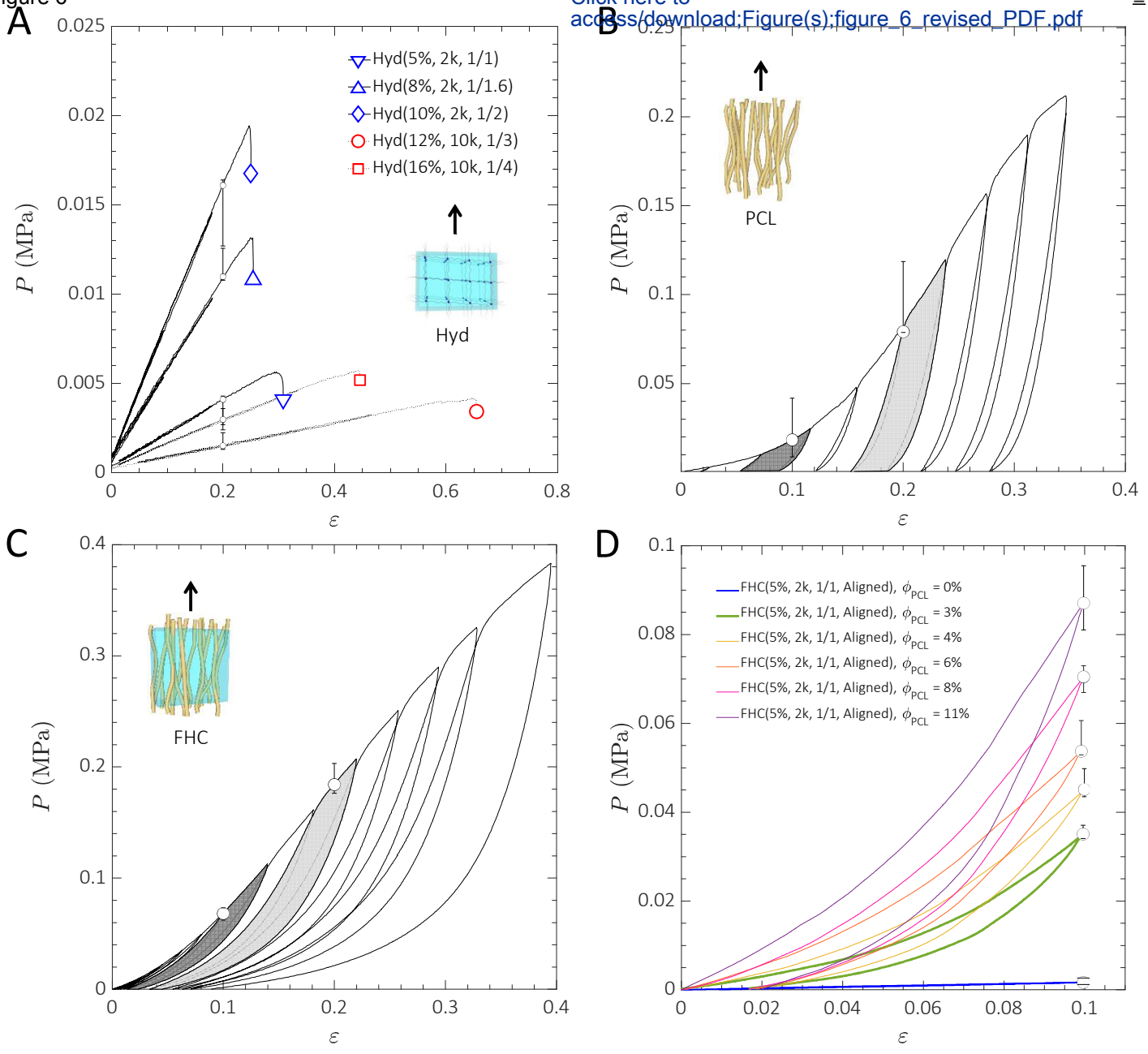

Figure 7

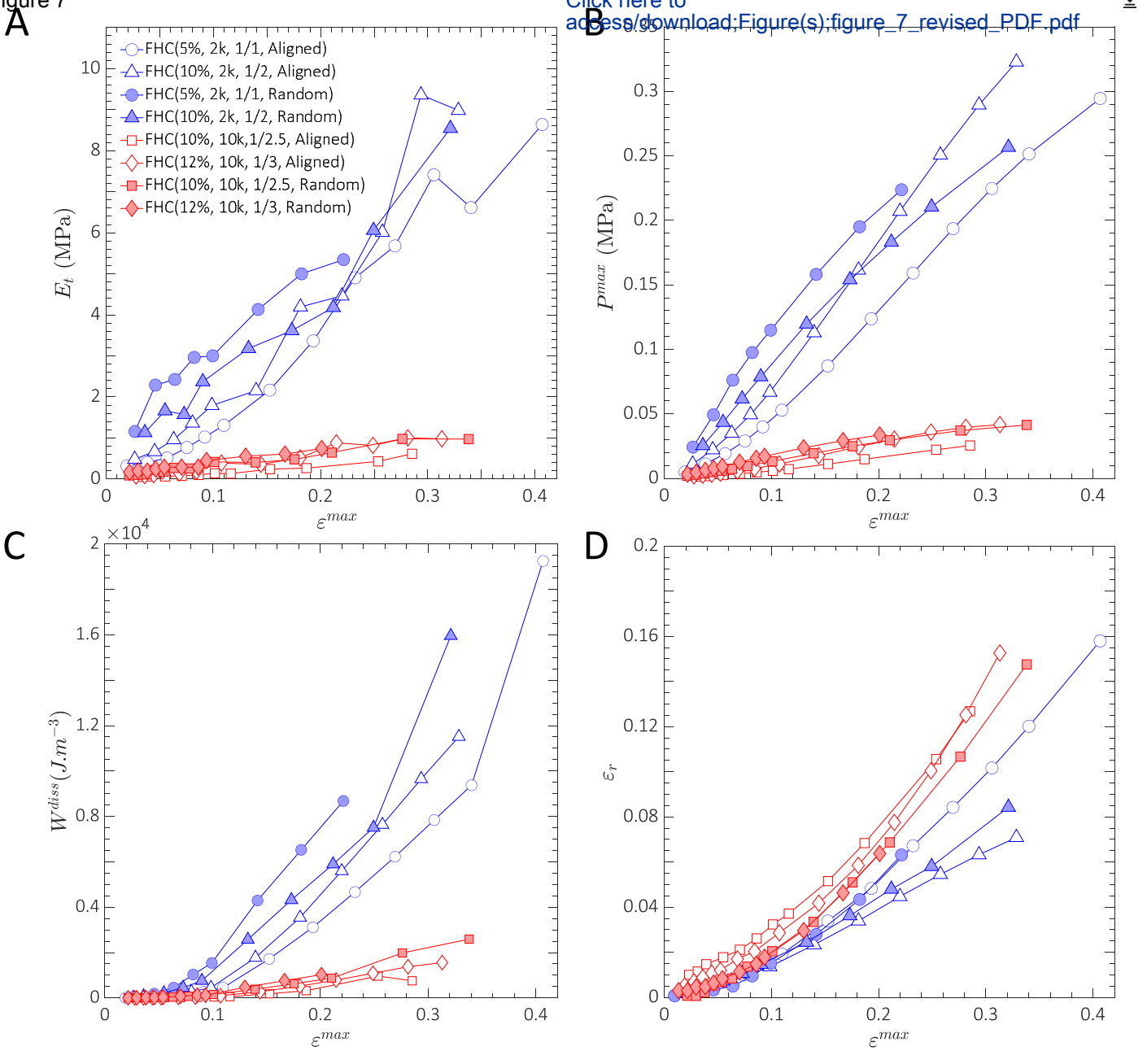

Figure 8

Click here to access/download;Figure(s);Figure_8_revised_PDF.pdf

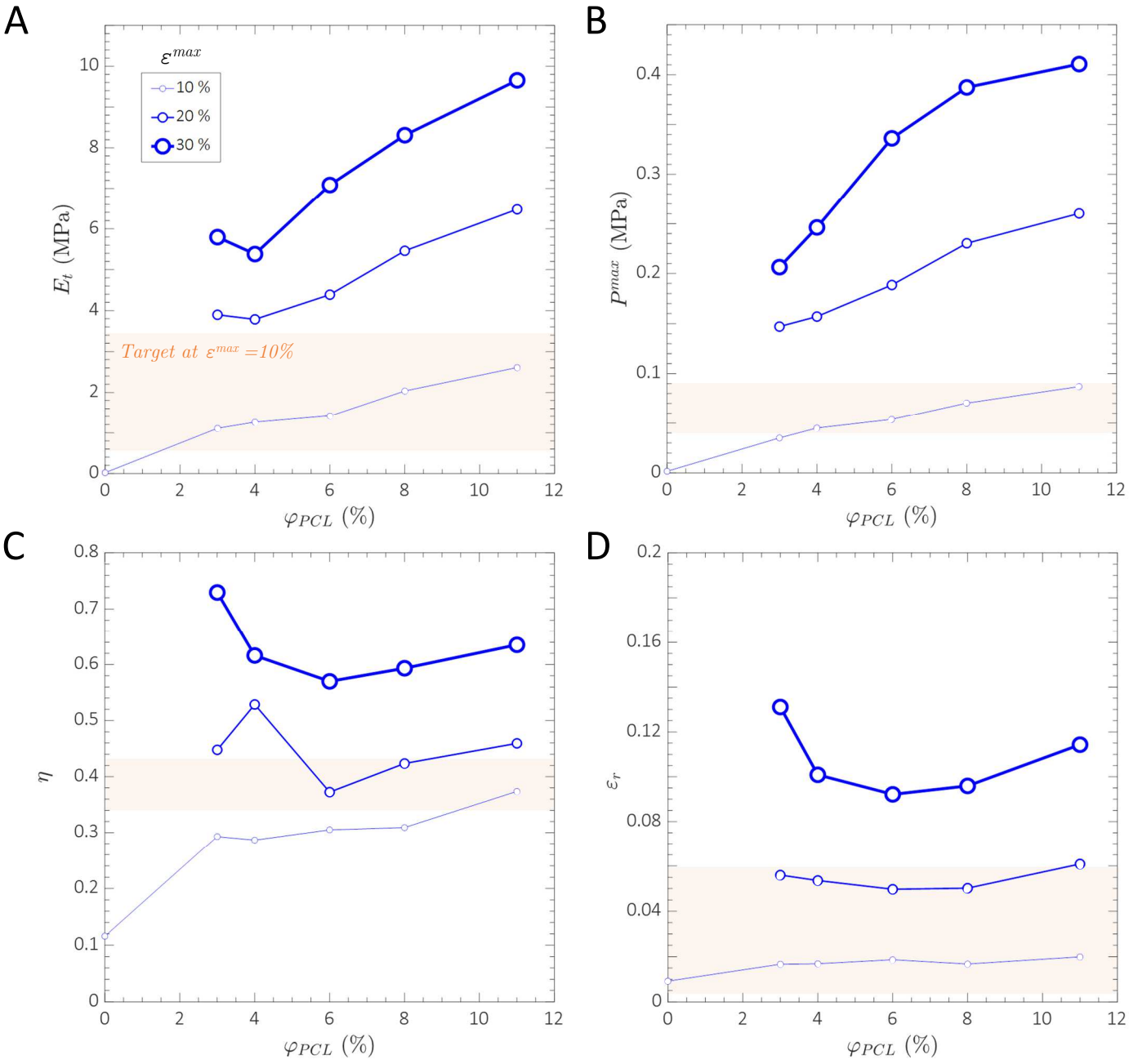

Figure 9

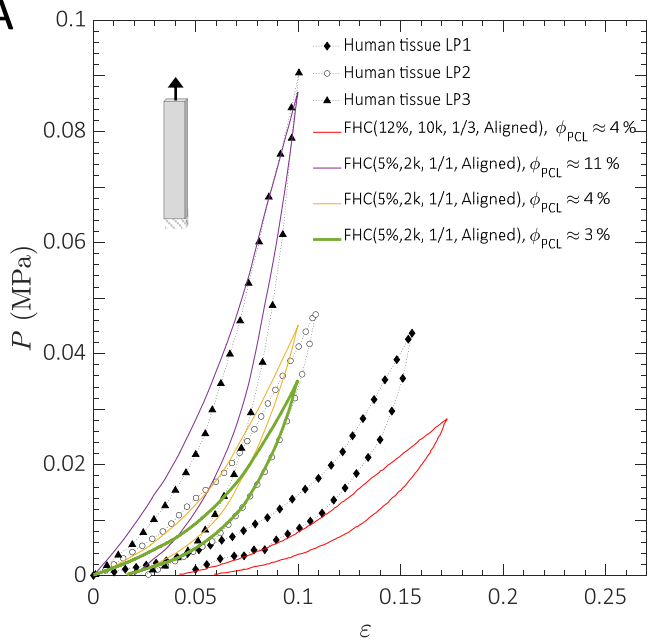

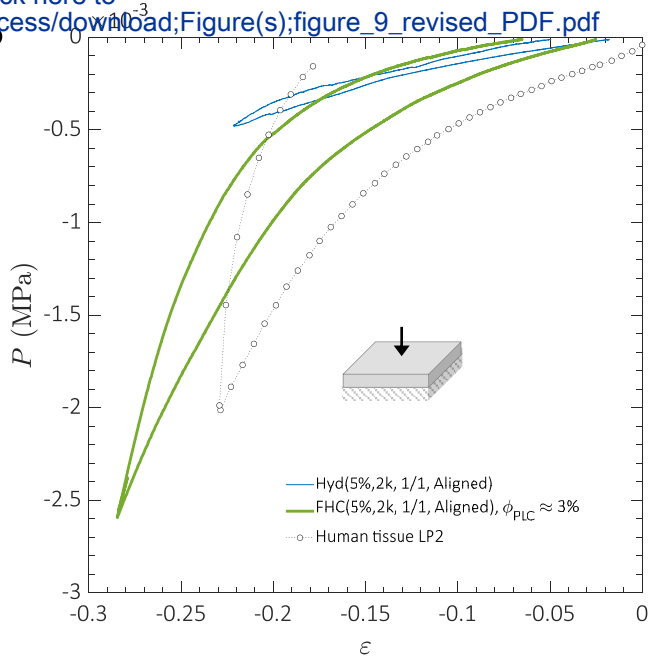

Table 1

DGL/PEG hydrogels	ζ ± SD (nm)	FHC composites	φ^{PCL} ± SD (%)
Hyd(5%, 2k, 1/1)	6.1 ± 0.2 ****	FHC(5%, 2k, 1/1, Random)	10.3 ± 0.7
		FHC(5%, 2k, 1/1, Aligned)	4.6 ± 0.1 ***
Hyd(10%, 2k, 1/2)	5.6 ± 0.3 ****	FHC(10%, 2k, 1/2, Random)	11.3 ± 0.5
		FHC(10%, 2k, 1/2, Aligned)	5.2 ± 0.5 ***
Hyd(10%, 10k, 1/2.5)	10.1 ± 0.4	FHC(10%, 10k, 1/2.5, Random)	7.4 ± 0.9
		FHC(10%, 10k, 1/2.5, Aligned)	3.4 ± 0.2 **
Hyd(12%, 10k, 1/3)	9.5 ± 0.6	FHC(12%, 10k, 1/3, Random)	8.1 ± 1
		FHC(12%, 10k, 1/3, Aligned)	3.7 ± 0.6 ***

Click here to access/download
Supplementary Material
Supplementary movie 1.mp4